Cyclin F drives proliferation through SCF-dependent degradation of the retinoblastoma-like tumor suppressor p130/RBL2

Taylor P Enrico[1,2], Wayne Stallaert[3], Elizaveta T Wick[1,2], Peter Ngoi[4], Xianxi Wang[2], Seth M Rubin[4], Nicholas G Brown[1,2], Jeremy E Purvis[2,3], Michael J Emanuele[1,2]*

[1]Department of Pharmacology. The University of North Carolina at Chapel Hill, Chapel Hill, United States; [2]Lineberger Comprehensive Cancer Center. The University of North Carolina at Chapel Hill, Chapel Hill, United States; [3]Department of Genetics. The University of North Carolina at Chapel Hill, Chapel Hill, United States; [4]Department of Chemistry and Biochemistry. University of California at Santa Cruz, Santa Cruz, United States

Abstract Cell cycle gene expression programs fuel proliferation and are universally dysregulated in cancer. The retinoblastoma (RB)-family of proteins, RB1, RBL1/p107, and RBL2/p130, coordinately represses cell cycle gene expression, inhibiting proliferation, and suppressing tumorigenesis. Phosphorylation of RB-family proteins by cyclin-dependent kinases is firmly established. Like phosphorylation, ubiquitination is essential to cell cycle control, and numerous proliferative regulators, tumor suppressors, and oncoproteins are ubiquitinated. However, little is known about the role of ubiquitin signaling in controlling RB-family proteins. A systems genetics analysis of CRISPR/Cas9 screens suggested the potential regulation of the RB-network by cyclin F, a substrate recognition receptor for the SCF family of E3 ligases. We demonstrate that RBL2/p130 is a direct substrate of SCF$^{\text{cyclin F}}$. We map a cyclin F regulatory site to a flexible linker in the p130 pocket domain, and show that this site mediates binding, stability, and ubiquitination. Expression of a mutant version of p130, which cannot be ubiquitinated, severely impaired proliferative capacity and cell cycle progression. Consistently, we observed reduced expression of cell cycle gene transcripts, as well a reduced abundance of cell cycle proteins, analyzed by quantitative, iterative immunofluorescent imaging. These data suggest a key role for SCF$^{\text{cyclin F}}$ in the CDK-RB network and raise the possibility that aberrant p130 degradation could dysregulate the cell cycle in human cancers.

*For correspondence:
emanuele@email.unc.edu

Editor's evaluation

The identification of the tumor suppressor RBL2/p130 as a substrate of cyclin F/SCF adds a new level of understanding about the role of this ubiquitin ligase in cell cycle control and identifies a novel functional interaction that could have implications for cancer. This work will be of interest to researchers in the fields of cell cycle and cancer biology.

Introduction

The eukaryotic cell cycle consists of a sequential progression of events that govern cell growth and division. During cell cycle progression, many hundred genes oscillate in expression, contributing to

myriad processes, including DNA replication, chromosome segregation, cytoskeletal organization, and so on. The expression of cell cycle genes is repressed during quiescence, a reversible state of growth arrest, and in early G1-phase, presenting a critical barrier to proliferation. The retinoblastoma protein (RB) is a vital regulator of cell cycle gene repression. During quiescence and in early G1-phase, RB binds and inhibits E2F transcription factors, repressing transcription of many cell cycle genes. RB is phosphorylated by Cyclin-Dependent Kinases 4 and 6 (CDK4/6), as well as CDK2 (*Narasimha et al., 2014*; *Rubin et al., 2020*). This phosphorylation causes RB to dissociate from E2F, promoting the E2F-dependent expression of cell cycle genes that catalyze S-phase entry and cell cycle progression (*Rubin et al., 2020*). Due to its critical role in restricting proliferation, RB is a prototypical tumor suppressor (*Dyson, 2016*).

RB has two closely related family members, RBL1/p107 and RBL2/p130 (*Dyson, 1998*; *Sadasivam and DeCaprio, 2013*). Both p107 and p130 are also tumor suppressors that prevent cell cycle gene expression by binding the repressor E2F proteins E2F4/5 (*Claudio et al., 1994*; *Zhu et al., 1993*), and both are also regulated by CDK-dependent phosphorylation (*Canhoto et al., 2000*; *Farkas et al., 2002*; *Hansen et al., 2001*). Additionally, p130 functions as part of the mammalian DREAM complex (<u>D</u>P, <u>R</u>B-like, <u>E</u>2F4/5, <u>a</u>nd <u>M</u>uvB) (*Litovchick et al., 2007*; *Smith et al., 1996*). DREAM assembles during quiescence and inhibits cell cycle progression by restricting the transcription of numerous cell cycle genes regulated by E2F, B-MYB, and FoxM1 transcription factors (*Fischer et al., 2016*; *Müller et al., 2012*). Accordingly, perturbations to p130 or the DREAM complex allow expression of its cell cycle target genes, shifting the balance from quiescence toward proliferation (*Forristal et al., 2014*; *Iness et al., 2019*; *Patel et al., 2019*).

RB and p130 collaborate to suppress proliferation. In mice, *Rb⁻/⁻p130⁻/⁻* mouse embryo fibroblasts (MEFs) grow more rapidly in culture than MEFs deficient in either *Rb* or *p130* alone, and *Rb⁻/⁻p130⁻/⁻* mice spontaneously form many more tumors than their respective single-gene knockouts (*Dannenberg et al., 2004*). In mouse models of small cell lung cancer, *p130* knockout increases tumor size and overall tumor burden, even in the background of *Rb* and *p53* loss (*Ng et al., 2020*; *Schaffer et al., 2010*). Consistent with its role as a tumor suppressor, *p130* cooperates with RB to repress G2-M genes in response to genotoxic stress (*Schade et al., 2019*). And, *p130* loss in primary human fibroblasts leads to increased expression of cell cycle genes compared to loss of *Rb* alone (*Schade et al., 2020*). These observations highlight the importance of p130 in cell cycle control, as well as its role in tumor suppression. These results also illustrate the importance of the broader CDK-RB network in normal proliferation, and the consequence of its dysregulation in the aberrant cell cycles observed in cancer. RB mutations, overexpression of cyclin D and cyclin E, loss of p130 protein, and dysregulation of the mammalian DREAM complex have all been implicated in increased cellular proliferation and tumorigenesis (*Forristal et al., 2014*). Interestingly, p130 mutations are infrequent compared to other tumor suppressors like *RB, CDKN2A*, and *p53*, suggesting the possibility that post-translational mechanisms could account for its inactivation.

Cyclin F is a non-canonical cyclin—it neither binds nor activates CDKs (*Bai et al., 1994*; *D'Angiolella et al., 2013*). Instead, cyclin F is one of ~70 F-box proteins, a family of substrate recognition receptors that recruit substrates to the Skp1-Cul1-Fbox protein (SCF) E3 ligase (*Bai et al., 1996*; *Cardozo and Pagano, 2004*). SCF ligases play an evolutionarily conserved role in promoting cell cycle progression by triggering the destruction of cell cycle inhibitors. For example, yeast SCF^Cdc4 and human SCF^Skp2 trigger the destruction of CDK inhibitors Sic1 and p27, respectively (*Carrano et al., 1999*; *Feldman et al., 1997*; *Schwob et al., 1994*; *Skowyra et al., 1997*).

Cyclin F mRNA and protein levels oscillate during the cell cycle, giving cyclin F cell cycle-dependent activity (*Bai et al., 1994*). Cyclin F begins to accumulate at the G1/S transition, peaks in G2, and its protein levels are subsequently downregulated via proteasomal degradation in mitosis and G1 (*Choudhury et al., 2016*; *Mavrommati et al., 2018*) where cyclin F is ubiquitinated by SCF^βTRCP following cyclin F phosphorylation by casein kinase II (*Mavrommati et al., 2018*). Cyclin F is also ubiquitinated by the cell cycle E3 Anaphase Promoting Complex/Cyclosome (APC/C) (*Choudhury et al., 2016*). Further, cyclin F has been implicated in the ubiquitination and degradation of several cell cycle proteins (*Emanuele et al., 2020*). Taken together, its dynamic regulation and substrate repertoire highlight the importance of cyclin F in cell cycle control.

We demonstrate here that cyclin F binds, ubiquitinates, and regulates the RB-family tumor suppressor p130. We identify the regions in both cyclin F and p130 that are required for their

interaction. Interfering with cyclin F-p130 regulation, by expressing a mutant version of p130 which cannot be ubiquitinated, causes a severe defect in proliferation. Taken together, these data implicate cyclin F as a new, key player in CDK-RB network regulation, highlighting a critical ubiquitin-based mechanism that controls cell proliferation.

Results

Cyclin F/CCNF fitness correlates with the CDK-RB network

The Project Achilles Cancer Dependency Map (DepMap) has performed near genome-wide, CRISPR/Cas9 loss-of-function screens in hundreds of cancer cell lines. Fitness scores, corresponding to each gene in each cell line, reflect the relative impact of individual gene knockout on proliferation and survival. Despite differences in protocols and reagents, DepMap scoring is highly concordant with Project Score, another large, pan-cancer, CRISPR/Cas9 screening platform (*Dempster et al., 2019*). Importantly, systems genetics analyses of these data can be used to identify physically or genetically linked genes/proteins, since their loss often similarly impact overall fitness (*Munoz et al., 2016*; *Boyle et al., 2018*; *Doench et al., 2016*; *Kory et al., 2020*; *McDonald et al., 2017*; *Pan et al., 2018*; *Wang et al., 2017*). The Pearson's correlation coefficient was computed for DepMap fitness gene scores across cell lines (17,634 genes in 789 cell lines at the time of analysis). This analysis effectively detects pathways involved in proliferation. For example, the gene most highly correlated with the DNA helicase component MCM2 is its complex member MCM4 (*Figure 1—figure supplement 1A*). The genes most highly correlated with mitogen-activated protein kinase MEK1/MAP2K1 are its upstream activator BRAF and its downstream effector ERK2/MAPK1 (*Figure 1—figure supplement 1A*). Genes that encode proteins in the Skp2-Cyclin E/A-CDK2-E2F pathway are highly correlated, as are those involved in autophagy (*Figure 1—figure supplement 1A*).

Fitness scores for those genes in CDK-RB network which promote proliferation (e.g., *CDK4*, *CCND1/Cyclin D1, etc.*) are well correlated between DepMap and Project Score (*Figure 1—figure supplement 2*; *Dempster et al., 2019*). The gene most highly correlated with *CDK4* is its coactivator *CCND1/Cyclin D1,* demonstrating that relevant genetic relationships in the CDK-RB network are correlated (*Figure 1—figure supplement 3A*). Interestingly, the ninth most highly correlated gene with *CDK4* was *CCNF*, which encodes cyclin F (*Bai et al., 1994*; *Bassermann et al., 2014*). *CCNF* is among the top 1% of highly correlated genes when analyzing several other members of the CDK-RB network, including *CDK4, CDK6, CCND1, and RBL1* (*Figure 1—figure supplement 3A*). Accordingly, when we determined those genes most highly correlated with *CCNF* knockout, *CDK4, CDK6, CCND1/Cyclin D1, RBL1,* and *RBL2* are among the top 85 genes, out of more than 17,630 (~0.5%; *Figure 1A*). Thus, the impact of *CCNF* knockout on fitness is highly correlated with genes in the CDK-RB network.

Gene ontology (GO) analysis on the top 94 genes correlated with *CCNF* (Pearson correlation >0.15) enriched GO terms related to cell cycle, regulation of ubiquitin protein ligase activity, mitotic G1-phase and G1/S transition, Cyclin D1-CDK4-CDK6 complex, G1/S specific transcription, and Cyclin A-CDK2 associated events at S-phase entry (*Figure 1B*). When we filtered the top *CCNF* correlated genes by the GO term 'cell division' (*Figure 1C*), three sub-networks emerged: the Nde1-kinetochore complex, the Anaphase Promoting Complex/Cyclosome (APC/C), and the CDK-RB network. Identification of eight subunits of the APC/C complex is consistent with our previous observation of a reciprocal relationship between SCF^cyclin F and APC/C^Cdh1 (*Choudhury et al., 2016*). Among the remaining genes/proteins were two known cyclin F substrates: *E2F7*, which encodes the transcriptional repressor E2F7 (*Yuan et al., 2019*), and *FZR1*, which encodes the APC/C coactivator protein, Cdh1 (*Choudhury et al., 2016*).

We examined endogenous proteins corresponding to CDK-RB network genes that correlate most strongly with *CCNF* using two breast cancer cell lines, MCF-7 and T47D, engineered for doxycycline-inducible expression of cyclin F (*Wasserman et al., 2020*). Cells were treated with increasing amounts of doxycycline for 24 hr, and immunoblotted for CDK4, CDK6, cyclin D1, p107, and p130. We observed a specific downregulation of endogenous p130 in both cell lines, whereas all other proteins remained unchanged (*Figure 1D*). Similarly, p130 levels decrease in a time-dependent manner following doxycycline treatment, and this can be prevented by inhibiting the proteasome with MG132, or cullin RING E3 ligases, using the neddylation inhibitor MLN4924 (*Figure 1—figure supplement 3B*; *Ohh et al.,*
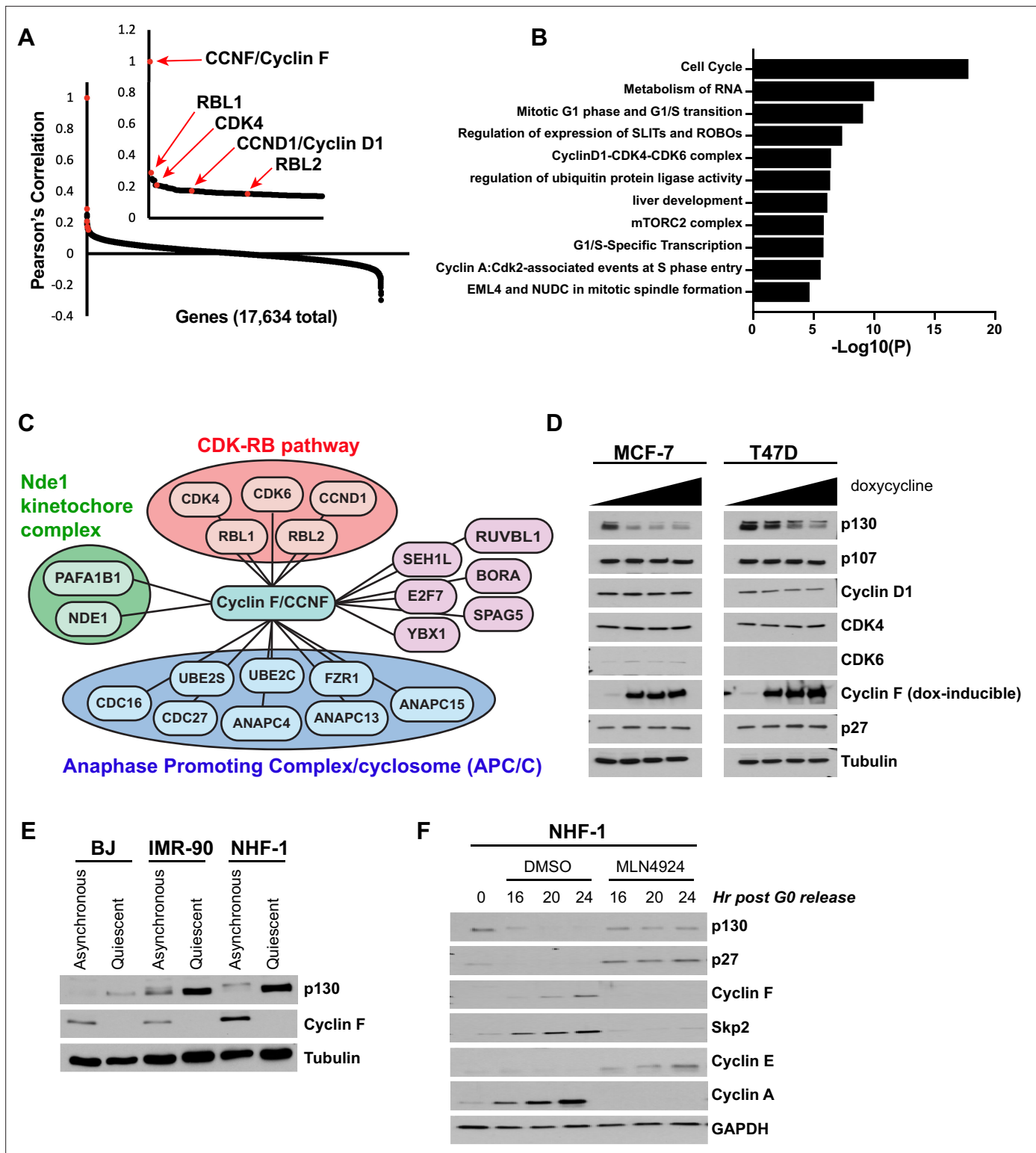
Figure 1. Analysis of the Cancer Dependency Map reveals that *CCNF* is highly correlated with the CDK-RB network. (**A**) Cancer Dependency Map data from project Achilles were analyzed to identify the impact of gene loss-of-function on cellular fitness, and fitness correlation with that of *CCNF,* based on pooled CRISPR/Cas9 gene knockout screens performed in 789 cell lines. Pearson's correlation coefficients are reported for all gene pairs (each dot corresponds to a single *CCNF*-gene X pair). The Pearson's correlations for *CCNF* compared to 17,634 other genes are shown. The CDK-RB network members highlighted in red all score in the top 0.5% of genes whose impact on fitness is most highly correlated with *CCNF.* (**B**) Gene ontology (GO) analysis was performed for the top 0.05% of genes whose impact on fitness is most highly correlated with *CCNF.* The top 10 enriched GO terms and

Figure 1 continued on next page

Figure 1 continued

their corresponding p-value is shown. (**C**) The top 0.05% of genes whose impact on fitness is most highly correlated with *CCNF* were sorted by the GO term cell division (GO:0051301). A graphical representation of the remaining 21 genes is shown. Genes are grouped by their known associations with specific functional pathways or complex, including CDK-RB, Nde1-kinetochore, or APC/C. (**D**) MCF-7 and T47D cells were engineered to contain a TET-inducible cyclin F transgene. Cells were treated with 0 (vehicle control), 5, 25, or 100 ng/ml of doxycycline to induce cyclin F expression, and the indicated proteins were analyzed by immunoblot. No band was detected for CDK6 in T47D cells. Representative of n=3 experiments. (**E**) BJ, IMR-90, and NHF-1 human fibroblast cell lines were synchronized in G0 by 48 hr serum starvation (quiescent) or allowed to proliferate normally (asynchronous). Whole-cell extracts were collected for immunoblot analysis. Representative of n=3 experiments. (**F**) NHF-1 cells were synchronized in G0 by serum starvation for 48 hr. Cells were then released into the cell cycle upon the addition of serum-containing media supplemented with either MLN4924 or vehicle (DMSO) as a control. Cells were collected at the indicated time points after release. Protein levels were assessed by immunoblot. Data represent n=3 independent experiments.

The online version of this article includes the following figure supplement(s) for figure 1:

Figure supplement 1. Analysis of Project Achilles Dependency Map reveals that highly correlated genes encode proteins known to interact.

Figure supplement 2. Gene dependency scores from the Broad Institute Project Achilles Dependency Map data set and the Sanger Project Score data set correlate highly.

Figure supplement 3. Analysis of Project Achilles Dependency Map reveals that *CDK-RB* network genes correlate highly with *CCNF*.

2002; *Soucy et al., 2009*). Taken together, these data suggest that cyclin F might regulate p130 degradation.

To further assess the relationship between cyclin F and p130, we compared asynchronous human fibroblasts to those same cells synchronized in quiescence by serum-starvation for 48 hr. In each of cell lines tested (BJ, IMR-90, and NHF-1), cyclin F protein levels significantly decrease in quiescence, whereas p130 protein levels increase, establishing an inverse expression pattern (*Figure 1E*). Next, NHF-1 cells were synchronized in quiescence by serum deprivation and then released into the cell cycle. Cyclin F protein began to accumulate as cells re-entered the cell cycle at G1/S, similar to what was previously reported (*Choudhury et al., 2017*; *D'Angiolella et al., 2012*; *Figure 1—figure supplement 3C*). Meanwhile, p130 was degraded as cells exited quiescence. The accumulation kinetics of cyclin F is similar to another F-box protein, Skp2, which ubiquitinates p27, marking it for degradation. Skp2 has also been implicated in p130 degradation (*Bhattacharya et al., 2003*; *Tedesco et al., 2002*). However, p130 has a different degradation pattern than p27, and in a previous study, p130 was still degraded in Skp2 knockout cells (*Tedesco et al., 2002*).

To determine whether the SCF and cullin E3 ligase family is required for p130 degradation at quiescence exit, we synchronized NHF-1 and T98G cells in quiescence and then released cells into the cell cycle in the presence of either DMSO (control) or MLN4924. In cells treated with MLN4924, neither p130 nor p27 is degraded, cyclin E accumulates but does not get degraded, and there is a significant delay in cyclin A accumulation (*Figure 1F* and *Figure 1—figure supplement 3D*).

To determine p130 levels in the absence of cyclin F, we first utilized *CCNF* knockout HeLa cells generated using CRISPR/Cas9 gene editing (*Choudhury et al., 2016*). In HeLa cells, p130 protein levels are higher in CCNF KO cells (sgCCNF) than in control cells (sgCTRL; *Figure 2A*). Next, CCNF KO and control HeLa cells were synchronized at G1/S by double thymidine block. After release, p130 levels were higher in the CCNF knockouts at every time point analyzed (*Figure 2—figure supplement 1A*). We then transiently depleted cyclin F from NHF-1 or IMR-90 cells. Cyclin F depletion increased p130 in both cell lines and with two different siRNAs (*Figure 2B*). Neither CCNF KO HeLa cells, nor the transiently depleted NHF-1 or IMR-90 cells, exhibited significant defects in overall cell cycle compared to their respective controls, judged by propidium iodide staining and analyzed by flow cytometry (*Figure 2—figure supplement 1B-D*). Consistent with the regulation of p130 by cyclin F resulting from a physical interaction, endogenous cyclin F co-immunoprecipitated endogenous p130 from HEK293T and U2OS cells (*Figure 2C*).

p130 degradation is proteasome- and neddylation-dependent and requires the canonical cyclin F substrate-binding site

We determined if exogenously expressed cyclin F affects the stability of exogenously expressed p130 protein. In HEK293T cells transfected with HA-tagged p130 (HA-p130), increasing amounts of FLAG-tagged cyclin F (FLAG-cyclin F) reduced p130 levels in a dose-dependent manner (*Figure 3A*).
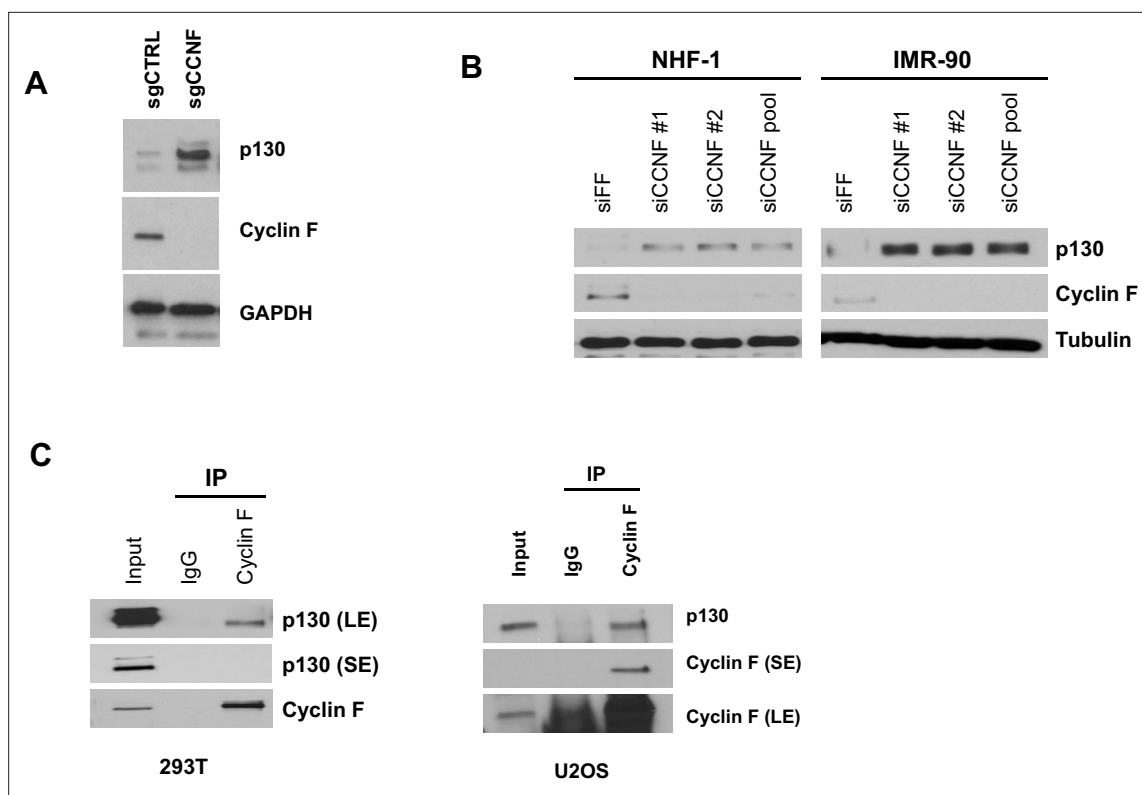
Figure 2. Cyclin F regulates and interacts with endogenous p130. (**A**) Asynchronously proliferating *CCNF* CRISPR/Cas9 knockouts (sgCCNF) and control (sgCtrl) HeLa cells were blotted for levels of the indicated proteins. Representative of n=3 experiments. (**B**) NHF-1 and IMR-90 cells were transfected with two different siRNAs targeting *CCNF* or a control siRNA targeting Firefly Luciferase (siFF). Whole-cell lysates were immunoblotted for the indicated proteins. Representative of n=3 experiments. (**C**) Endogenous cyclin F was immunoprecipitated from asynchronously proliferating HEK293T cells (left) or asynchronously proliferating U2OS cells (right). Indicated proteins were immunoblotted. SE=short exposure; LE=long exposure; representative of n=3 experiments.

The online version of this article includes the following figure supplement(s) for figure 2:

Figure supplement 1. Cyclin F knockout and depletion across cell lines.

Four human SCF E3 ligases are involved in marking substrates for degradation to promote entry and progression through S-phase: SCF$^{\text{cyclin F}}$, SCF$^{\text{Skp2}}$, SCF$^{\beta\text{TRCP}}$, and SCF$^{\text{Fbxw7}}$. We therefore transiently expressed HA-p130 alone or together with cyclin F, Skp2, Fbxw7, βTRCP1, or βTRCP2, and in both HEK293T and U2OS cells. p130 levels decreased only upon co-expression with cyclin F and not with any of the other F-box proteins (*Figure 3B* and *Figure 3—figure supplement 1A*).

In HEK293T cells, the reduction in HA-p130 caused by FLAG-cyclin F expression is reversed by addition of MG132 or MLN4924 (*Figure 3C*). Cyclin F recognizes its substrates through a hydrophobic patch motif in its cyclin domain (sequence MRYIL at amino acids M309-L313). Previous studies have shown that mutating the methionine and leucine residues to alanine (Cyclin F M309A L313A) can impair cyclin F binding to substrates (*Choudhury et al., 2016*; *D'Angiolella et al., 2012*; *D'Angiolella et al., 2010*). Notably, whereas cyclin F (WT) robustly downregulated p130 protein levels, cyclin F (M309A L313A) was unable to promote p130 degradation (*Figure 3D*). These data suggest that p130 is a cyclin F substrate.

p130 is a cyclin F substrate

Cyclin F recognizes Cy Motifs in substrates, which corresponds to the amino acid sequence RxL/I (where x=any amino acid)(*Choudhury et al., 2016*; *D'Angiolella et al., 2012*; *D'Angiolella et al., 2010*). There are 13 putative Cy motif sequences in p130 that span the length of the protein. We therefore created six HA-tagged p130 truncations, while considering p130 domain structure (*Figure 4A*). We transiently expressed each HA-p130 truncation alone, or together with FLAG-cyclin F (WT) and included conditions with and without proteasome and neddylation inhibitors. p130 degradation
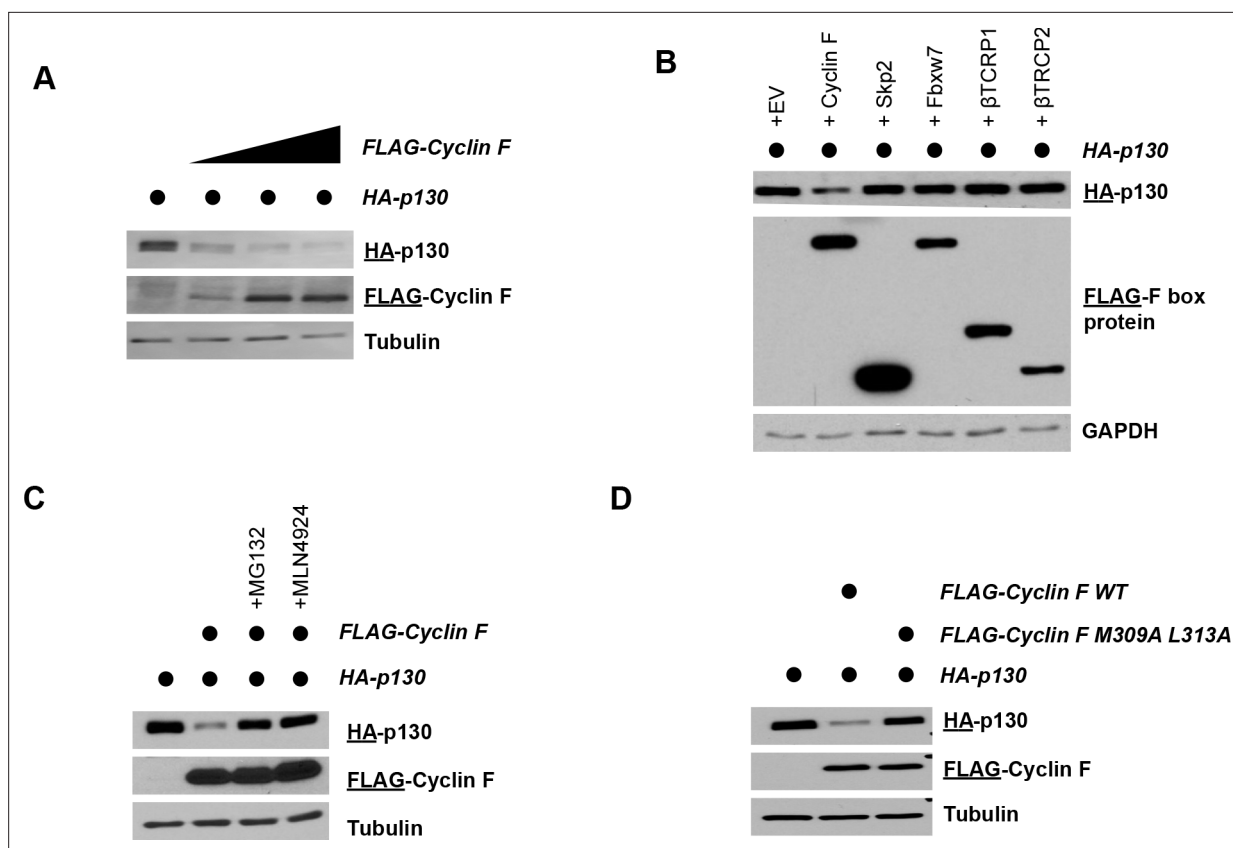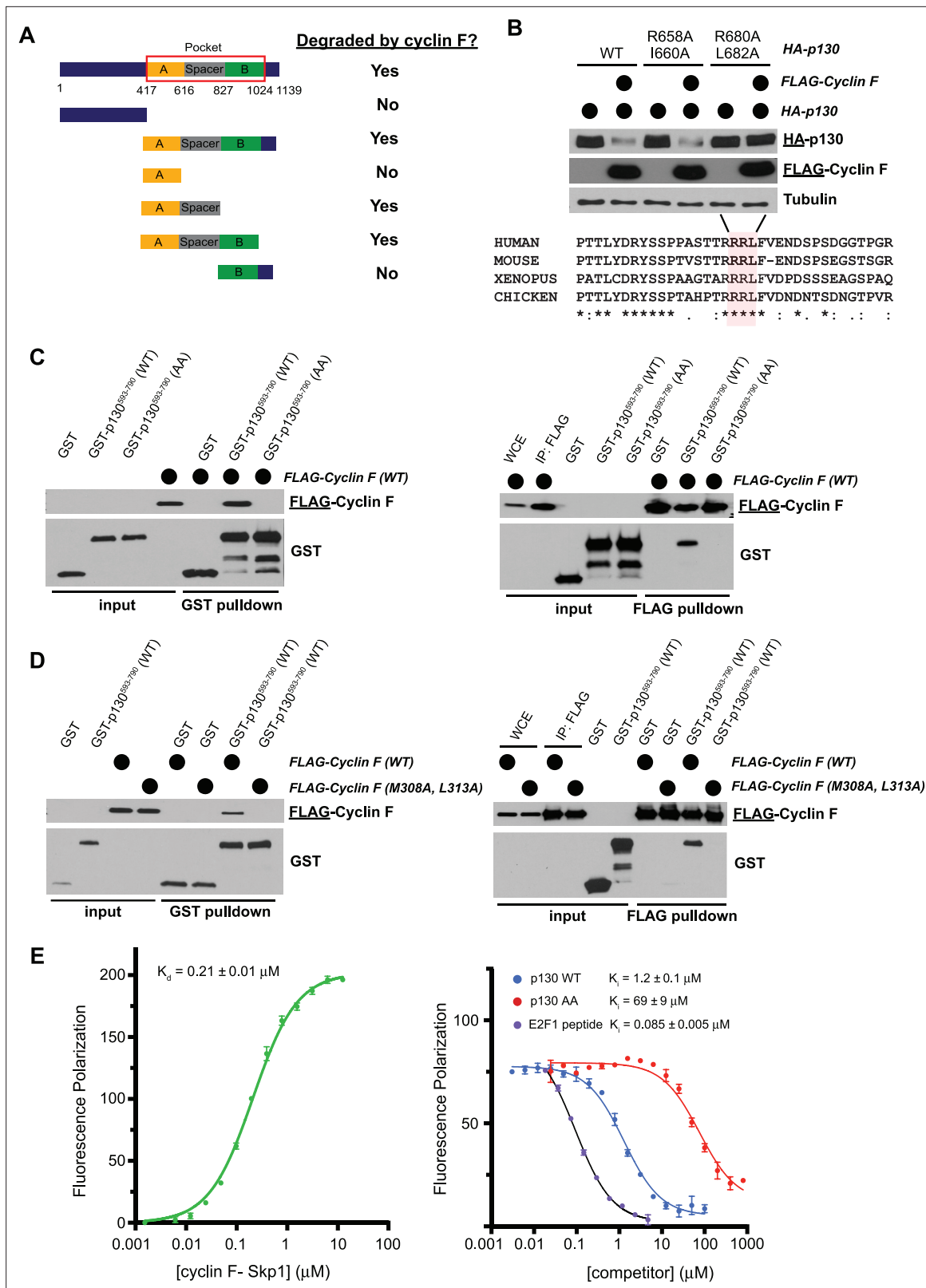
Figure 3. Cyclin F promotes p130 degradation. (**A**) HEK293T cells transiently expressing HA-p130 with an empty FLAG vector control (lane 1) or together with increasing amounts of FLAG-cyclin F (lanes 2–4). Cells were collected and analyzed by immunoblot 24 hr post-transfection. The antigen being immunoblotted for is represented by the underline, here and in all experiments below. Representative of n=3 experiments. (**B**) HEK293T cells transiently expressing HA-p130 with an empty FLAG vector control (lane 1) or together with FLAG-cyclin F (lanes 2–4). MG132 (proteasome inhibitor) or MLN4924 (neddylation inhibitor) were added for 6 hr prior to harvesting. Cells were collected and analyzed by immunoblot 24 hr post-transfection. Representative of n=3 experiments. (**C**) HEK293T cells transiently expressing HA-p130 with an empty FLAG vector control (lane 1) or together with FLAG-cyclin F WT (lane 2) or FLAG-cyclin F(M309A L313A) (lane 3), as indicated. Cells were collected and analyzed by immunoblot 24 hr post-transfection. Representative of n=3 experiments. (**D**) HEK293T cells transiently expressing HA-p130 with an empty FLAG vector control (lane 1) or together with the indicated FLAG-tagged F-box proteins (lanes 2–6). Cells were collected and analyzed by immunoblot 24 hr post-transfection. Representative of n=3 experiments.

The online version of this article includes the following figure supplement(s) for figure 3:

Figure supplement 1. P130 levels following Fbox protein expression in U2OS cells.

depended on the presence of a flexible spacer region, located between regions A and B in the p130 pocket domain (*Figure 4A*, *Figure 4—figure supplement 1A*). Within the spacer, there are two RxL/I motifs: R658-I660 and R680-L682. We mutated the first and last amino acid in each motif to alanine (AxA) in full-length HA-p130. Only the p130 (R680A L682A) mutant was resistant to cyclin F mediated degradation, demonstrating that these two amino acids alone are required for cyclin F to trigger p130 degradation (*Figure 4B*). That sequence and many surrounding residues are conserved in p130 proteins found in other species, including clawed frogs (*Xenopus tropicalis*), chickens (*Gallus gallus*), and mice (*Mus musculus*) (*Figure 4B*).

Since p130(R680A L682A; hereafter referred to as p130(AA)) cannot be degraded by cyclin F, we asked whether it still binds to cyclin F. GST-tagged p130 truncations were purified from *Escherichia coli* (amino acids 593–790; hereafter referred to as GST-p130), and mixed with total lysates from HEK293T cells expressing FLAG-cyclin F. In a GST-pulldown assay, FLAG-cyclin F bound to GST-p130(WT), but not to GST-p130(AA) or GST alone (*Figure 4C*, left panel). Conversely, FLAG-cyclin F, purified from HEK29T cells precipitated GST-p130(WT) but not GST-p130(AA) (*Figure 4C*, right panel). Consistent with its inability to trigger p130 degradation, cyclin F(M309A L313A) could not bind to GST-p130

Figure 4. Cyclin F binds p130 directly and promotes p130 degradation through a conserved degron motif. (**A**) Graphical depiction of p130 domain structure. Indicated p130 truncation mutants were screened for their ability to be degraded following co-overexpression with cyclin F. The data supporting these conclusions are shown in *Figure 4—figure supplement 1*. (**B**) The first and last amino acids in the two potential cyclin F binding sites in the p130 spacer domain (R658-I660 and R680-L682) were mutated to alanine (AxA). HEK293T cells transiently expressed HA-p130 alone (WT or AxA

Figure 4 continued on next page

mutants, as indicated) or together with FLAG-cyclin F WT. Cells were collected and analyzed by immunoblot 24 hr post-transfection. Representative of n=3 experiments (top) and amino acid sequence alignment for human, mouse, frog, and chicken p130 (bottom). (C) GST-p130$^{593–790}$ (WT) and GST-p130$^{593–790}$ (AA) were produced in *Escherichia coli* and purified. FLAG-cyclin F was transiently expressed in HEK293T cells. GST pulldowns (left) and FLAG pulldowns (right) were used to determine the interaction of p130 and cyclin F. Interaction was assessed by immunoblot after pulldown (representative of n=3 experiments). (D) GST-p130(WT) and FLAG-cyclin F(WT) or FLAG-cyclin F(M309A L313A) were expressed as described in (C). Interaction and binding were assessed as in (C) (representative of n=3 experiments). (E) Fluorescence polarization anisotropy assay to detect direct association of p130 with cyclin F. (Left) 10 nM TAMRA-p130$^{674–692}$ probe was titrated with increasing concentrations of purified GST-cyclin F$^{25–546}$-Skp1. (Right) The p130 probe bound with 0.5 μM GST-cyclin F$^{25–546}$-Skp1 was displaced with increasing concentrations of the indicated p130 protein construct or E2F1$^{84–99}$ peptide. Experiments were performed in triplicate, and the standard deviation is reported as the error.

The online version of this article includes the following figure supplement(s) for figure 4:

Figure supplement 1. Requirements for cyclin F binding and degradation of p130 in vivo and in vitro.

(*Figure 4D*). Thus, the p130 Cy motif at R680-L682 and the cyclin F hydrophobic patch (M309-L313) are required for the p130-cyclin F interaction and for p130 degradation.

To assess the direct binding and affinity of p130 for cyclin F, we developed a fluorescence polarization anisotropy assay using a peptide containing the relevant Cy motif in p130. We used a version of cyclin F, produced in Sf9 cells, which lacks the first ~25 amino acids and its C-terminal PEST domain to improve solubility (cyclin F$^{25–546}$). We titrated recombinant, purified cyclin F$^{25–546}$-Skp1 dimer into a solution of synthetic, TAMRA-labeled, p130 peptide (residues 674–692) and observed a K_d of 0.21±0.01 μM (*Figure 4E*, left panel). Binding was efficiently competed away using purified GST-p130(WT) protein but not using GST-p130(AA), which had >50-fold higher K_i in the competition assay (*Figure 4E*, right panel). We found that an unlabeled E2F1 peptide containing the relevant Cy motif (residues 84–99), which was previously shown to mediate cyclin F-E2F1 association (*Clijsters et al., 2019*), also competed with the p130 probe. We performed a similar competition assay using a TAMRA labeled E2F1$^{84–99}$ peptide as a probe, and we found that we could efficiently compete the E2F1 peptide with GST-p130(WT) but not GST-p130(AA) (*Figure 4—figure supplement 1B*). We conclude that p130 directly binds cyclin F-Skp1 at a site that overlaps with the E2F1 binding site and that the association is dependent on critical interactions made by R680 and L682 in p130.

To analyze p130 ubiquitination, we reconstituted the SCF$^{cyclin F}$ ubiquitination reaction in vitro using purified components. Cyclin F$^{25–546}$ was combined with neddylated Cul1-Roc1(Rbx1), Skp1, substrate, and ubiquitin. The human homolog of ariadne (ARIH1) is a RING-Between-RING (RBR) E3 ligase that has been shown to work with the E2 UBCH7 and other cullin ring E3 ligases, including the SCF, to ubiquitinate substrates (*Horn-Ghetko et al., 2021*; *Scott et al., 2016*). Therefore, ARIH1/UBCH7 and the chain-elongating E2 CDC34B were used as the ubiquitin transfer module.

SCF$^{Cyclin F}$ robustly ubiquitinated GST-p130(WT) (*Figure 5A*). This modification was dependent on the inclusion of NEDD8-Cul1-Roc1, Skp1-Cyclin F, and ARIH1/UBCH7, since the exclusion of any of these components completely abrogated ubiquitination (*Figure 5A*). Significantly, GST-p130(AA) was unable to be ubiquitinated by SCF$^{cyclin F}$.

Because cyclin F can ubiquitinate p130(WT), we determined the stability of p130(WT) and p130(AA) in the absence or presence of cyclin F. To determine p130 half-life, we expressed full-length HA-p130(WT) or HA-p130(AA) with or without FLAG-cyclin F in HEK293T or U2OS cells for 24 hr. Cells were treated with the protein synthesis inhibitor cycloheximide (CHX) and then analyzed for HA-p130 half-life. While p130(WT) half-life was significantly reduced by ectopic expression of cyclin F, p130(AA) remained stable for the length of the experiment in the presence or absence of cyclin F (*Figure 5B–C* and *Figure 5—figure supplement 1A*), indicating that protein levels of p130(AA) are resistant to cyclin F-mediated degradation.

We asked whether p130(AA) accumulates more than p130(WT) during a specific cell cycle phase. To evaluate p130 levels at different points during the cell cycle, we first engineered NHF-1 cells to express HA-tagged p130(WT) or p130(AA) in response to doxycycline treatment (*Figure 5—figure supplement 1B*). NHF-1 cells expressing p130 were synchronized with vehicle control, aphidicolin (S-phase synchronization), or nocodazole (Mitosis synchronization) for 16 hr. Interestingly, p130(WT) levels are decreased in nocodazole-synchronized cells compared to p130(AA) levels (*Figure 5D*). Consistently, nocodazole synchronization significantly decreased endogenous p130 protein levels in
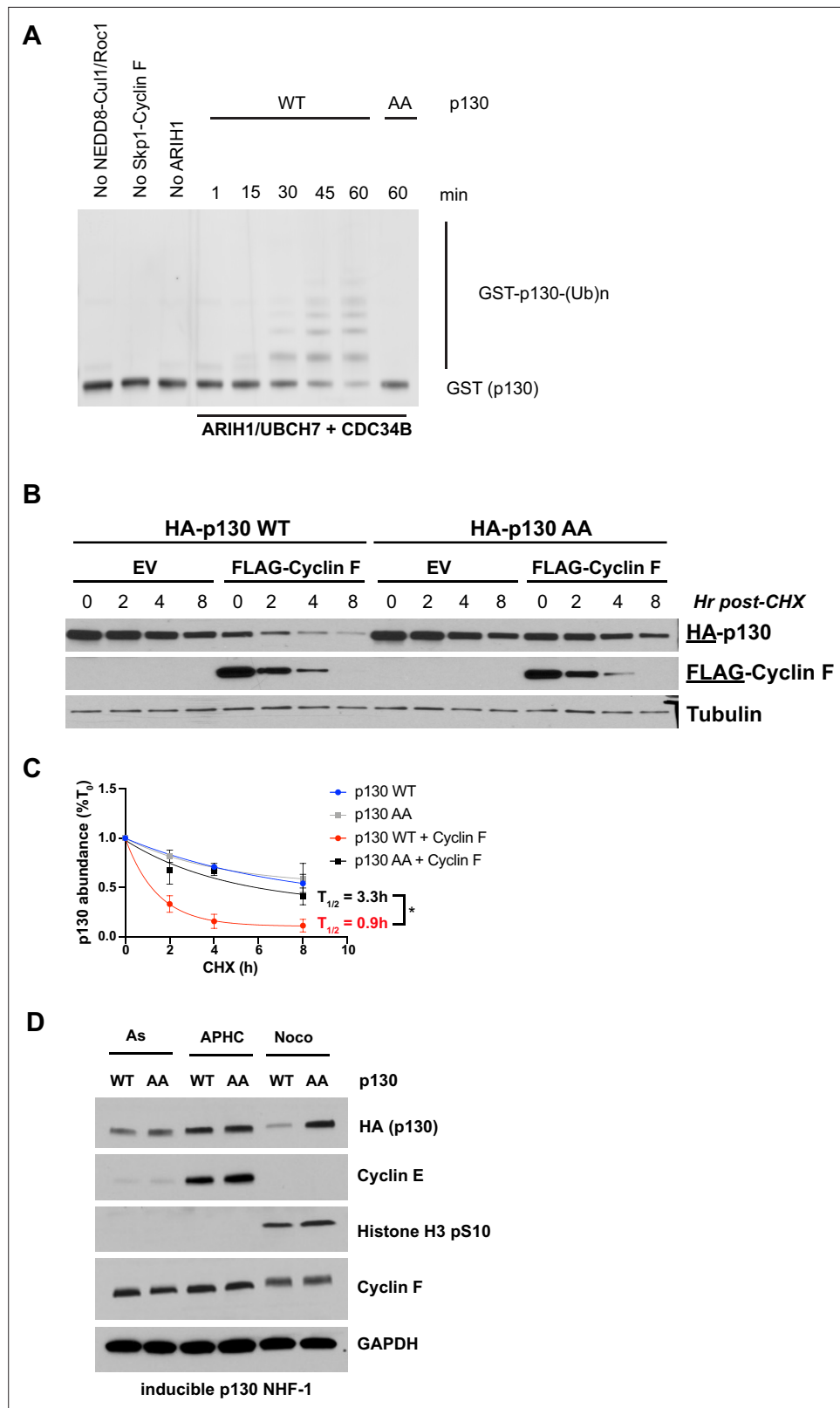
Figure 5. SCF[Cyclin F] regulates the ubiquitination and stability of p130. (**A**) Ubiquitination reactions were performed with SCF[cyclin F], ARIH1/UBCH7, and CDC34B. GST-tagged p130[593–790] WT and GST-p130[593–790] were used as substrates and detected by immunoblot against GST. Data are representative of n=3 experiments. (**B**) FLAG-cyclin F, HA-p130(WT), and/or HA-p130(AA) were transiently expressed in HEK293T cells for 24 hr. The protein synthesis

Figure 5 continued on next page

Figure 5 continued

inhibitor cycloheximide (CHX) was added and cells were collected at the indicated time points. Protein levels were determined by immunoblot. Representative of n=3 experiments. (**C**) Quantification of (**B**). *=p<0.05 (Student's t-test). Data are shown as mean ± SEM for n=3 experiments. (**D**) Inducible p130 NHF-1 cells were grown in media-containing 100 ng/ml doxycycline for 14 days to induce p130 expression, or in media-containing vehicle control. On indicated days, cells were pulsed with EdU for 30 min prior to harvest/fixation, DNA was stained with DAPI, and cells were analyzed by flow cytometry. Data for S- and G2/M phases are in *Figure 6—figure supplement 1D*. Data represent mean ± SEM for n=3 replicates.

The online version of this article includes the following figure supplement(s) for figure 5:

Figure supplement 1. p130 stability in U2OS and NHF-1 cells.

Figure supplement 2. Both p130(WT) and p130(AA) can be phosphorylated and can associate with cyclin E, cyclin A, the DREAM complex, Large T antigen, and E7 protein.

NHF-1 cells (*Figure 5—figure supplement 1C*). Taken Together, these data indicate that p130(WT) levels decrease in nocodazole synchronized NHF-1 cells, whereas levels of p130(AA) remain stable.

The Cy motif that we mapped at amino acids 680–682 was previously implicated in binding cyclins A and E in SF9 cell extracts (*Lacy and Whyte, 1997*). To evaluate binding in human cells, we utilized the NHF-1 cells engineered to express p130(WT) or p130(AA). We immunoprecipitated (IP) HA and found that similar amounts of cyclin A and E co-purify with HA-p130(WT) and HA-p130(AA) (*Figure 5—figure supplement 2A*). Reciprocally, following IP of endogenous cyclin A, both HA-p130(WT) and HA-p130(AA) co-immunoprecipitated (*Figure 5—figure supplement 2B*). Further, we assessed whether mutation of the p130 Cy motif would impair p130 phosphorylation. HA-tagged p130(WT) and p130(AA) immunoprecipitated from NHF-1 cells are similarly phosphorylated on the CDK site at S672 (*Figure 5—figure supplement 2C*). Additionally, HA-p130(WT) and HA-p130(AA) migrate similarly in SDS-PAGE, their migration was similarly increased by post-lysis phosphatase treatment with calf intestinal phosphatase (CIP), and this could be prevented by the addition of phosphatase inhibitors (*Figure 5—figure supplement 2D*). These findings are consistent with previous reports mapping additional cyclin E and A binding sites to sequences in the p130 amino-terminus, and cyclin D binding to a carboxy-terminal helix (*Castaño et al., 1998*; *Hansen et al., 2001*; *Topacio et al., 2019*). Further, HA-tagged p130(WT) and p130(AA) can associate with the DREAM complex based on the co-IP of Lin54 following an HA pulldown (*Figure 5—figure supplement 2C*). Finally, we determined that the Cy motif mutations did not impact p130 binding to large T-antigen in HEK293T cells or the E7 oncoprotein in HeLa cells (*Figure 5—figure supplement 2E-F*).

Loss of P130 regulation by cyclin F causes G0/G1 arrest and apoptosis

Interfering with RB phosphorylation, by expression of a mutant harboring substitutions at CDK phosphorylation sites, impairs cell cycle progression (*Fry et al., 2004*; *Lukas et al., 1997*). To similarly isolate the phenotypic impact of cyclin F on p130, independent of other substrates, we utilized the NHF-1 cells engineered with a doxycycline inducible expression of p130(WT) or p130(AA) (*Figure 5—figure supplement 1A*). To determine whether p130(AA) accumulates more than p130(WT), we collected cells at various time points after induction. Although protein levels of p130(WT) and p130(AA) are initially equal, p130(AA) accumulated to higher levels compared to p130(WT) over time (*Figure 6A*), consistent with p130(AA) being resistant to degradation.

To assess proliferation, we induced expression of low levels of p130(WT) or p130(AA) and allowed cells to proliferate in culture for 14 days. Cells were split regularly, provided fresh media supplemented with doxycycline every 48 hr, and never reached confluency. Expression of non-degradable p130(AA) led to a profound decrease in proliferation/viability based on a PrestoBlue assay (*Figure 6—figure supplement 1A*). After 14 days, the PrestoBlue signal was decreased 5.8-fold (~83%) in p130(AA)-expressing cells relative to p130(WT) controls.

Next, we directly quantified proliferation by counting cells every 48 hr for 2 weeks after p130(WT) or p130(AA) induction. The p130(AA)-expressing cells proliferated much more slowly than the p130(WT)-expressing cells (*Figure 6B*). After 14 days, there were 7.7-fold (~87%) less cells in the p130(AA) population compared to p130(WT)-expressing controls. The average doubling time was 33 hr for p130(WT)-expressing cells and 48 hr for p130(AA)-expressing cells (*Figure 6C*). As a control, both cell lines were treated with vehicle alone. There was no difference in proliferation across a 2-week
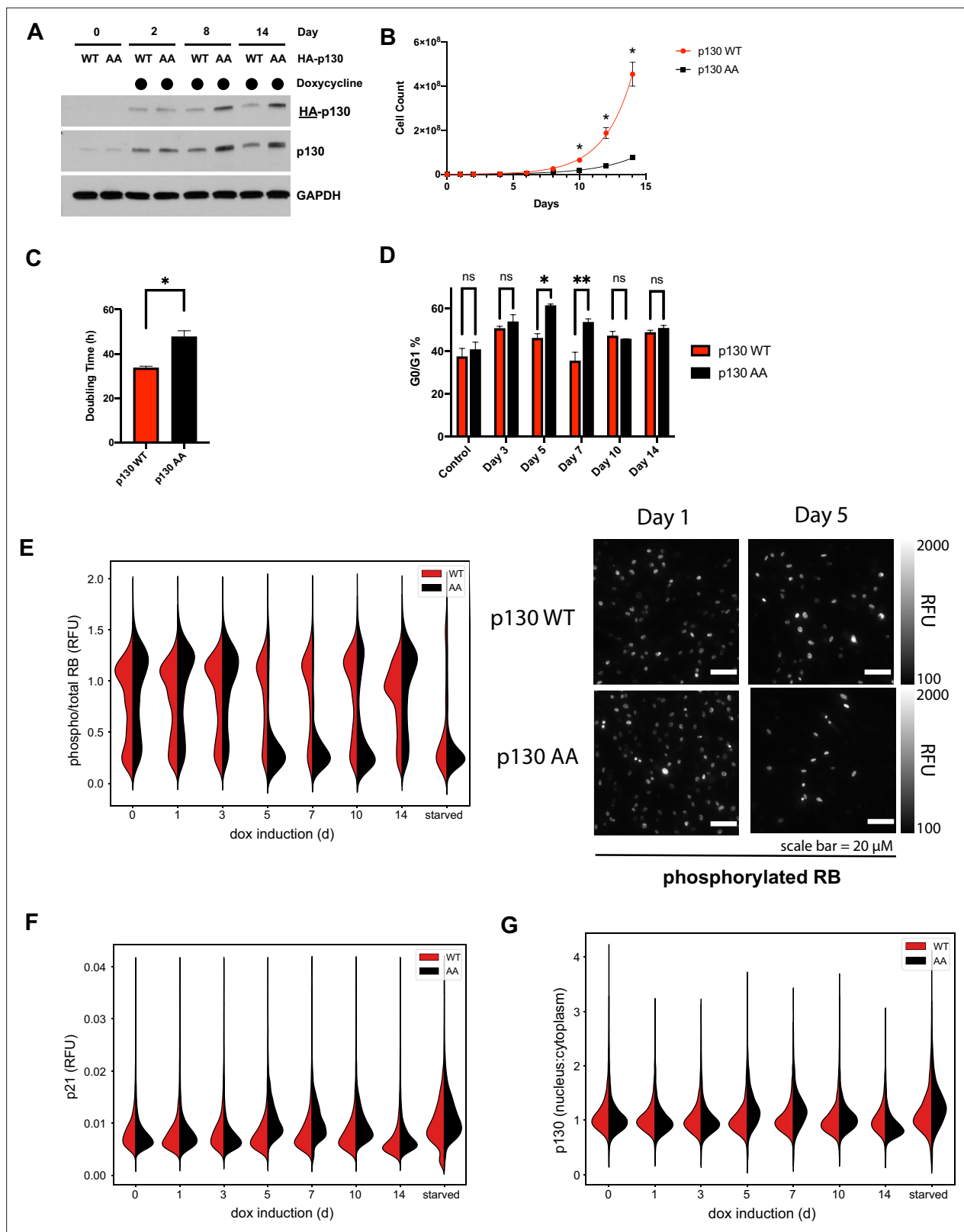
Figure 6. Cells expressing p130(AA) exhibit proliferation defects. (**A**) NHF-1 cells were engineered to express a TET-inducible HA-p130(WT) or HA-p130(AA) transgene. Doxycycline (100 ng/ml) was used to induce p130 expression, and water was used as a vehicle control. HA-p130 levels were assessed by immunoblot after cells were grown in doxycycline for up to 14 days. (**B**) Inducible p130 NHF-1 cells were grown in 100 ng/ml doxycycline-containing media for 14 days to induce p130 expression. Cells were counted on the indicated days. Data represent mean ± SEM for n=3 independent

Figure 6 continued on next page

Figure 6 continued

experiments. (**C**) Doubling time was calculated from counting experiment in (**B**). Error bars are SEM for n=3 independent experiments. Representative of n=2 independent experiments. (**D**) NHF-1 cells were grown in media supplemented with nocodazole for 16 hr, then immunoblotted for the indicated proteins. Representative of n=2 independent experiments. (**E–G**) Inducible p130 NHF-1 cells were grown in 100 ng/ml doxycycline for indicated times. Cells were fixed and analyzed by iterative immunofluorescent staining and imaging. Distributions of single-cell measurements are shown for nuclear phosphorylated versus total RB (**E**, left) and representative images of phosphorylated RB are shown for indicated days (**E**, right). Distributions of single-cell measurements are also shown for cytoplasmic p21 (**F**) and nuclear versus cytoplasmic p130 (**G**), as indicated.

The online version of this article includes the following figure supplement(s) for figure 6:

Figure supplement 1. TET-inducible p130(WT) and p130(AA) NHF-1 cells proliferate rapidly prior to induction of p130 expression.

Figure supplement 2. Cell cycle distribution and p130 staining from 4i experiments.

experiment (***Figure 6—figure supplement 1B-C***). Expectedly, ectopic expression of p130(WT) slowed the doubling time compared to cells treated with vehicle, consistent with previous studies which report p130 overexpression slows cell growth (***Lacy and Whyte, 1997***). However, p130(AA) had a much more severe impact on proliferation/survival.

We investigated whether the slow growth observed following p130(AA)-induction resulted from cell cycle arrest. We performed flow cytometry to analyze cell cycle phase distribution using EdU incorporation and DNA staining. NHF-1 were pulsed with EdU for 30 min prior to fixation at several time points after p130 induction. Total DNA was stained with DAPI, and cells were analyzed by flow cytometry. The percent of p130(AA)-expressing cells in G0/G1 significantly increased at days 5 and 7 compared to p130(WT)-expressing cells, while the percentage of S-phase cells was significantly decreased (***Figure 6D*** and ***Figure 6—figure supplement 1D***). Surprisingly, beyond day 10, there was no difference in G0/G1% between p130(AA) and p130(WT)-expressing cells, suggesting that the cell population may adapt to the increased levels of p130, which remain elevated throughout the entire 2-week experiment (***Figure 6D***).

We used iterative indirect immunofluorescence imaging (4i) to determine the levels of cell cycle markers in p130(WT)- and p130(AA)-expressing cells. 4i is accomplished by repeated antibody staining, followed by imaging, stripping, and re-staining, that collectively produce a set of targeted protein measurements in single cells. The resulting images are 'stacked' to quantify the expression of multiple proteins and antigens across an identical set of individual cells (***Gut et al., 2018***). Automated and semi-automated methods are used to identify cell boundaries and extract quantitative protein-level information for each cell (***Gut et al., 2018***).

To determine whether cells were arresting in G1, we stained for total and phospho-RB. RB is phosphorylated in proliferating cells, while unphosphorylated RB is a hallmark of G1/G0. RB phosphorylation was decreased in p130(AA)-expressing cells at days 5, 7, and 10 compared to p130(WT)-expressing cells or vehicle-treated controls (***Figure 6E***). We also found that p21 was increased in p130(AA)-expressing cells at days 5, 7, and 10, consistent with a G0/G1 arrest (***Figure 6F***). To assess cell cycle distribution in each population, we quantified total DNA content. DNA content analysis revealed that a larger percentage of p130(AA)-expressing cells had <4C DNA content compared to p130(WT)-expressing cells at days 5, 7, and 10, consistent with cells accumulating in G0/G1-phase (***Figure 6— figure supplement 2A***). Finally, we assessed the subcellular localization of p130 at each time point by quantifying the ratio of nuclear:cytoplasmic intensity from immunofluorescence images. We found p130(AA) was more localized to the nucleus at days 5 and 7 compared to p130(WT) (***Figure 6G*** and ***Figure 6—figure supplement 2B***), consistent with p130(AA) mediating cell cycle arrest through cell cycle gene repression.

As a component of the DREAM complex, p130 functions to prevent the transcription of myriad early (S-phase) and late (G2/M) cell cycle genes (***Engeland, 2018***). Because we observe an increase in G0/G1% for populations of cells expressing p130(AA), we sought to determine the expression levels of several DREAM target genes including: *CCNF, CCNE1, CDC6, DHFR, E2F1, and CDT1*. There was a significant reduction in expression of all of these in p130(AA)-expressing cells compared to those expressing p130(WT) (***Figure 7A***). Since both p130(WT)-expressing cells and p130(AA)-expressing cells grew more slowly than cells not expressing a p130 transgene, we also performed RT-qPCR on control cells; the expression of *CCNF, CCNE1, CDC6, DHFR, E2F1, and CDT1* was lower in both p130(WT)- and p130 (AA)-expressing cells compared to controls (***Figure 7—figure supplement 1A***). Thus, ectopic expression of p130 reduces transcription of DREAM target genes, which is further
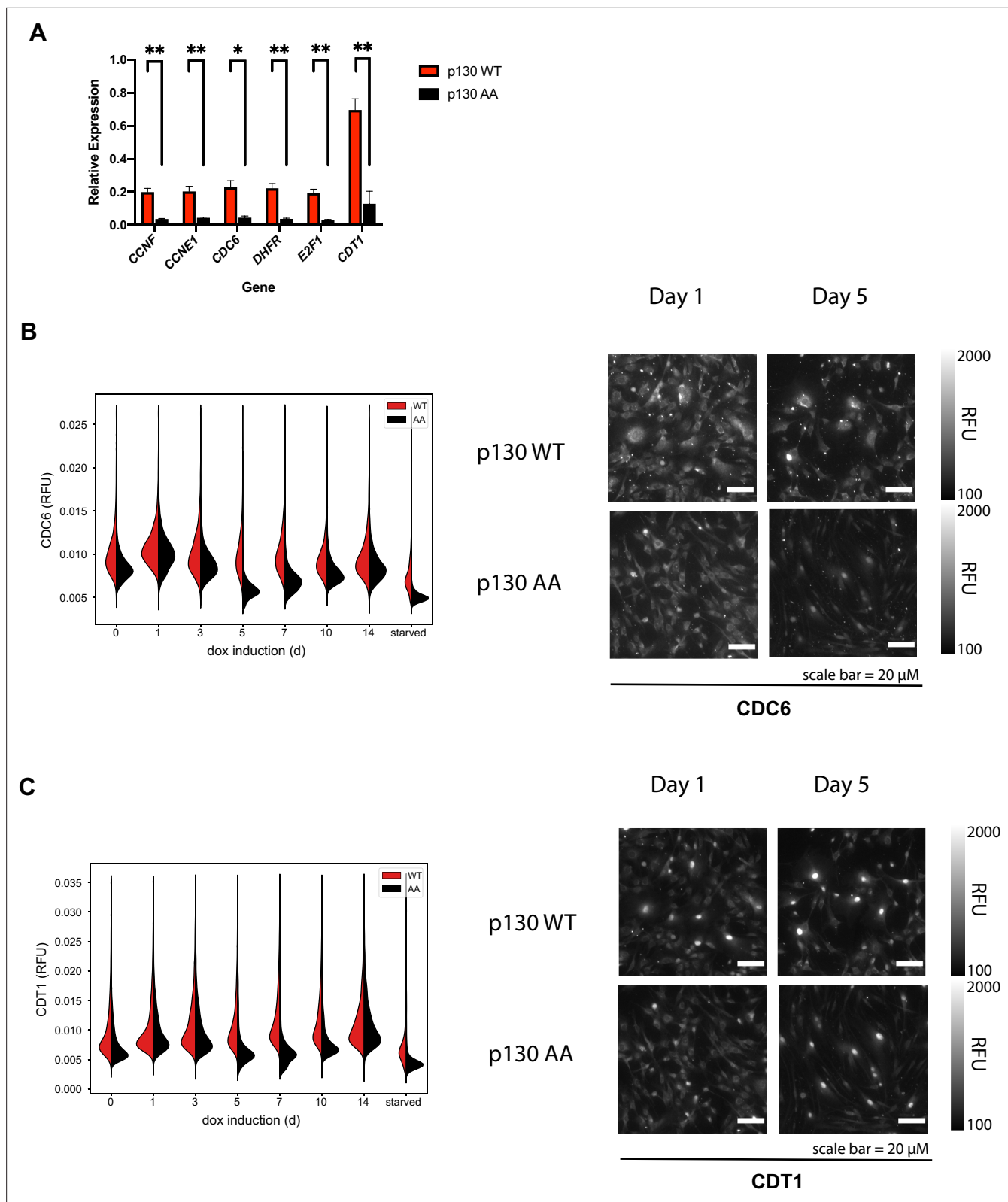
Figure 7. DREAM targets are downregulated in cells expressing p130(AA). (**A**) Inducible p130(WT) and p130(AA) NHF-1 cells were grown for 8 days in media-containing 100 ng/ml doxycycline to induce p130 expression. RNA was extracted for rt-qPCR analysis. Gene expression is relative to GAPDH expression and normalized to the vehicle control. Data are mean of n=3 experiments, and error bars are SEM. (**B, C**) Inducible p130 NHF-1 cells were grown in 100 ng/ml doxycycline for indicated times, and protein levels of CDC6 (**B**) and Cdt1 (**C**) were analyzed by iterative immunofluorescent staining

Figure 7 continued on next page

decreased by the expression of p130(AA). To confirm that the reduction in gene expression of DREAM targets led to decreased protein expression, we used 4i to quantify two DREAM targets by immuno-fluorescence: CDC6 and Cdt1. Consistent with DREAM activation, as well as observed G0/G1 arrest, protein levels of both CDC6 and Cdt1 were decreased from days 5 to 10 in p130(AA)-expressing cells compared to p130(WT)-expressing cells (*Figure 7B–C*).

Because not all cells arrest in G0/G1, we asked whether another factor may also be contributing to the reduced proliferation of the p130(AA)-expressing population. High p130 levels have previously been linked to apoptosis (*Pentimalli et al., 2018*; *Ventura et al., 2018*), whereas low p130 levels have been shown to protect against apoptosis (*Bellan et al., 2002*). We therefore examined the apoptotic markers cleaved PARP and cleaved caspase 3. As a positive control, cell lines were treated with 100 nM staurosporine to induce apoptosis. We observe cleaved PARP in the p130(AA)-expressing population at days 7, 10, and 14, and cleaved caspase 3 at days 7 and 10, indicating that cells in these populations are undergoing apoptosis. We did not observe cleaved PARP or cleaved caspase in any of the populations for p130(WT)-expressing cells (*Figure 7—figure supplement 2A*). Additionally, we performed flow cytometry for Annexin V and propidium iodide incorporation in unfixed cells to assess apoptosis/necrosis. We observed a higher percentage of apoptotic/necrotic cells in the p130(AA)-expressing population compared to the p130(WT)-expressing population at day 8 (*Figure 7—figure supplement 2B*). Since DNA damage can cause apoptosis, and because high p21 levels can be an indicator of DNA damage, we used 4i to determine the expression of proteins in the DNA damage response pathway, including 53BP1, phospho-Chk1, and phospho-H2A.X. We found that in the p130(AA)-expressing cells at days 5, 7, and 10, that levels of 53BP1, phospho-Chk1, and phospho-H2A.X were down-regulated (*Figure 7—figure supplement 2C-E*). A decrease in DNA damage markers is consistent with fewer cells being in S-phase and suggests that DNA damage is not the cause of apoptosis. We also examined senescence but saw no apparent increase in beta-galactosidase staining in p130(AA)-expressing cells.

Discussion

We demonstrate that the RB-like protein p130 is a substrate of the E3 ubiquitin ligase SCF$^{Cyclin\ F}$. Cyclin F loss allows p130 to accumulate, whereas its overexpression promotes p130 degradation. Cyclin F and p130 bind directly, and SCF$^{cyclin\ F}$ can ubiquitinate p130 in a fully reconstituted in vitro system. We mapped a critical cyclin F binding motif in p130, and when that sequence is mutated, it prevents p130 ubiquitination and degradation. This mutant version of p130 accumulates in normal human fibroblast cells, causing slowed proliferation, an accumulation in G0/G1-phase, and apoptosis.

Taken together, our results suggest that cyclin F contributes to inactivation of p130 and is therefore a regulator of the CDK-RB network. This finding is consistent with our observation that *CCNF* KO is correlated with *CDK4* and *CCND1/Cyclin D1* KO (*Figure 1—figure supplement 3*). Interestingly, the DepMap has tested hundreds of cell lines for their sensitivity to over 1000 oncology and non-oncology drugs. We queried these data for gene-drug similarities related to the selective CDK4/6 inhibitors Palbociclib and Ribociclib, which are used to treat metastatic, hormone receptor positive breast cancer (*Agostinetto et al., 2021*; *Kay et al., 2021*). Comparing Palbociclib to CRISPR knockout screens, revealed *CCND1/Cyclin D1 and CDK4* as the most highly correlated genes, validating this approach. Notably, *CCNF* ranked ninth among over 17,000 genes queried (*Figure 8A*). For Ribociclib, *CCND1* is the most highly correlated, *CDK4* is ranked 5th, and *CCNF* was 125th, falling within the top 1% of most highly correlated genes (*Figure 8B*). Conversely, we determined which drugs are highly correlated with *CDK4, CCND1, and CCNF* KO. Palbociclib and Ribociclib are among the top four most highly correlated drugs with *CDK4* and *CCND1* (*Figure 8C–D*). Remarkably, when *CCNF/Cyclin*
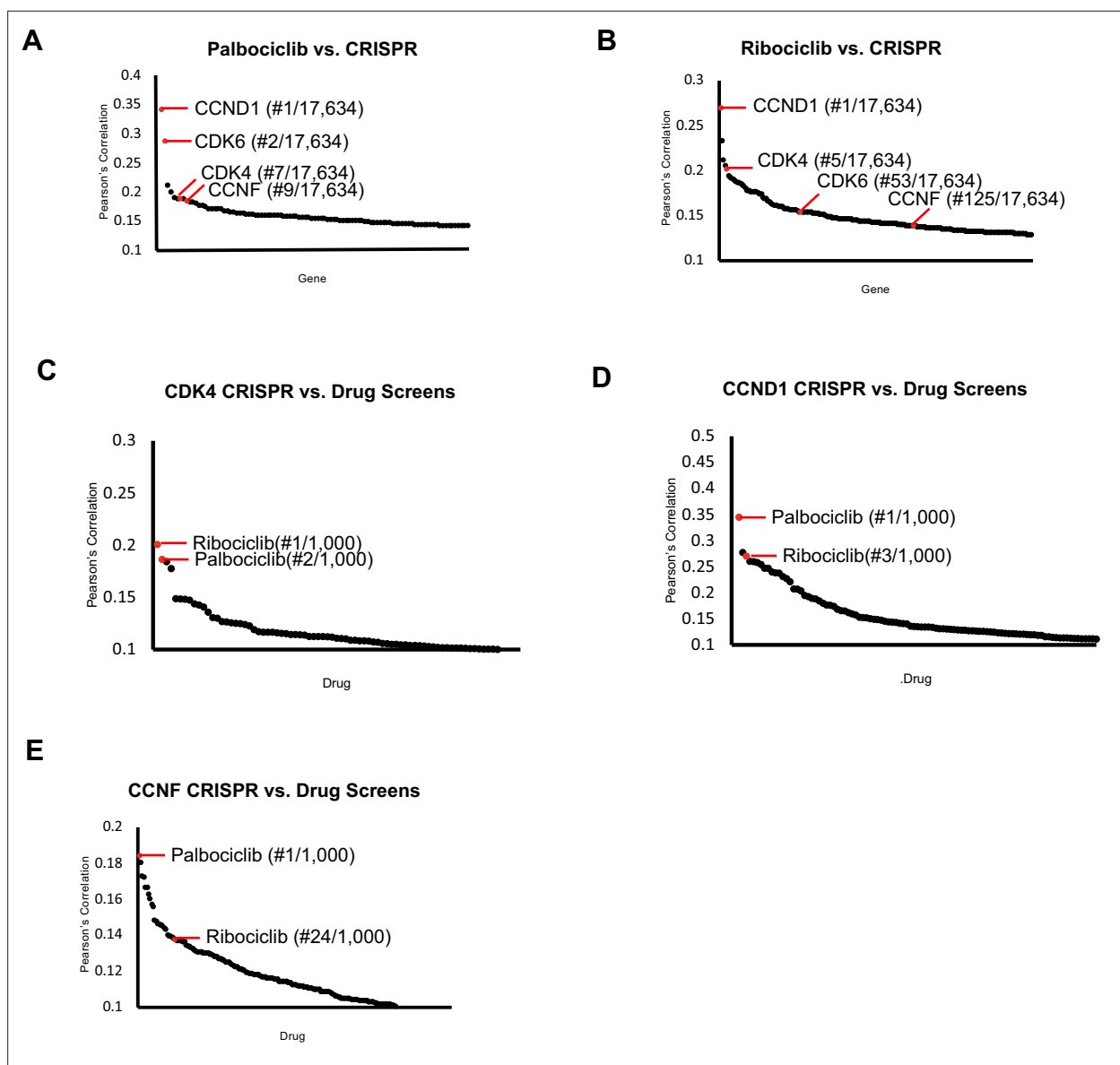
Figure 8. CDK4/6 inhibitors and CCNF knockout correlate highly. Project Achilles Dependency Map data sets were analyzed to determine: (**A**) Pearson's correlation coefficients for gene knockout correlated with Palbociclib treatment. (**B**) Pearson's correlation coefficients for gene knockout correlated with Ribociclib treatment. (**C**) Pearson's correlation coefficients for the correlation between *CDK4* knockout and 1000 drug treatments. (**D**) Pearson's correlation coefficients for the correlation between *CCND1* knockout and 1000 drug treatments. (**E**) Pearson's correlation coefficients for the correlation between *CCNF* knockout and 1000 drug treatments. For (**A–E**), only the top scoring, most statistically significant associations are shown.

F knockout is compared to all drugs tested, Palbociclib is ranked 1st, and Ribociclib is ranked 24th (***Figure 8E***). Thus, *CCNF* KO is highly correlated with both genetic and pharmacologic inactivation of the CDK-RB network across hundreds of cell lines.

RB-family protein dynamics throughout the cell cycle

The activity of RB and the RB-like proteins, p107 and p130, oscillates during the cell cycle and quiescence. Cyclin-CDK complexes phosphorylate RB, p107, and p130, which prevents their binding to activator E2Fs, allowing for the transcription of cell cycle target genes. In addition, RB-like proteins are also controlled at the level of their abundance. As cells exit quiescence, p130 protein is degraded by the ubiquitin-proteasome system. Then, when cells transition from proliferation to quiescence, p130 protein levels significantly increase (***Smith et al., 1996***). The role of phosphorylation in controlling RB and the RB-like proteins has been well-established (***Canhoto et al., 2000***; ***Farkas et al., 2002***;

Hansen et al., 2001); however, much less is known about how changes in the levels of RB-like proteins might contribute to changes in pathway activity or their ability to restrain E2F transcription factors. Notably, as cells grow bigger, RB and its yeast ortholog Whi5, are diluted, contributing to cell cycle progression (*Schmoller et al., 2015*; *Zatulovskiy et al., 2020*). Our studies suggest that the targeted degradation of p130 by cyclin F, which rapidly reduces its concentration, also plays a significant role in promoting cell cycle progression.

Despite a concrete understanding of the role of phosphorylation in regulating RB-like proteins, less is known about the role of ubiquitin ligases. The phosphatase subunit NRBE3 was previously linked to RB ubiquitination (*Wang et al., 2015*). A nucleolar protein, U3 protein 14a (hUTP14a), was also suggested to be a novel type of E3 ubiquitin ligase, capable of promoting both RB and p53 degradation and cancer cell proliferation (*Liu et al., 2018*). However, neither NRBE3 nor hUTP14a are ubiquitin ligases. Finally, RB degradation by an unknown, Cul2-based E3 was shown in cells expressing HPV E7 oncoprotein (*White et al., 2012*). Previous studies have reported that SCF^{Skp2} recognizes p130 and promotes its ubiquitination (*Bhattacharya et al., 2003*; *Tedesco et al., 2002*). However, p130 still cycles in Skp2 knockout cells, suggesting additional E3 ligase(s) may be involved in p130 regulation. Surprisingly, for unknown reasons, Skp2 overexpression had no effect on p130 levels in our experiments.

Cyclin F as a regulator of the cell cycle gene transcription

Cyclin F has previously been linked to cell cycle gene transcription via its regulation of several proteins, including B-MYB, SLBP, E2F1, E2F2, E2F3a, E2F7, and E2F8 (*Emanuele et al., 2020*). In response to DNA damage, cyclin F is able to bind to B-MYB, and rather than ubiquitinate it, inhibits the ability of B-MYB to promote the expression of mitotic genes (*Klein et al., 2015*). In G2, cyclin F ubiquitinates the stem-loop binding protein (SLBP), which is required during S-phase to mediate histone biogenesis (*Dankert et al., 2016*). Also, during G2, cyclin F catalyzes the ubiquitination of the activator E2Fs: E2F1, E2F2, and E2F3a (*Burdova et al., 2019*; *Clijsters et al., 2019*). The ubiquitination of activator E2Fs allows for their degradation, and expression of mutant E2Fs that can no longer bind to cyclin F results in increased expression of E2F target genes. Further, during G2-phase, cyclin F was shown to regulate the atypical repressor E2Fs, E2F7, and E2F8, promoting their degradation (*Wasserman et al., 2020*; *Yuan et al., 2019*). Each of these substrates implicates cyclin F in indirectly controlling cell cycle gene expression, and our study uncovers a new mechanism by which cyclin F regulates transcriptional control at the start of the cell cycle, by ubiquitinating p130.

Adding to the complexity of the role of cyclin F in cell cycle transcription, not only does cyclin F regulate p130 degradation, but p130 regulates the expression of cyclin F. Thus, cyclin F and p130 appear to exist in a double negative feedback loop, where each can downregulate the other. Interestingly, in response to DNA damage, cyclin F is downregulated by degradation (*D'Angiolella et al., 2012*), and p130 has been suggested to become activated to repress cell cycle gene expression. Thus, the degradation of cyclin F in response to genotoxic stress could preserve cell cycle arrest by allowing for the accumulation of p130, while also contributing to increased nucleotide pools through the accumulation of another cyclin F substrate, RRM2 (*D'Angiolella et al., 2012*).

Effect of P130 overexpression on proliferation

We have shown that expressing the mutant p130(AA), but not p130(WT), causes growth arrest and apoptosis. These results are consistent with clinical observations of outcomes of p130 expression levels in cancerous tissues. In lung cancers, p130 expression negatively correlates with histological grading and metastasis (*Baldi and Esposito, 1997*). For endometrial cancer patients who receive surgery, low p130 levels are significantly associated with increased recurrence and death (*Susini et al., 1998*). In vulvar carcinomas, loss of p130 and p27 has been shown to contribute to carcinogenesis (*Zamparelli et al., 2001*). In oral squamous cell carcinoma, p130-negative cases have worse prognoses than p130-positive cases (*Tanaka et al., 2001*). And, finally, in thyroid neoplasms, reduced p130 expression has been linked to the aggressive characteristics of anaplastic carcinoma, while high p130 expression in micropapillary carcinoma has been linked to the smaller size of those tumors (*Ito et al., 2003*). Thus, cancers with low p130 expression or p130 loss, seem to grow more quickly and aggressively, whereas cancers with high p130 expression are correlated with better prognoses. Our findings fit within the context of these studies; as p130(AA) accumulates, the cells are less proliferative and some die by

apoptosis. Since p130 mRNA levels are not regulated during the cell cycle, it is interesting to speculate that enhancing p130 degradation in some malignancies could contribute to defects in the regulation of cell cycle gene expression and hyper-proliferation. Likewise, blocking p130 degradation could phenocopy CDK4/6 inactivation and could potentially be therapeutically advantageous, and would be consistent with our analysis showing that loss-of-function in cyclin D, CDK4, and cyclin F are highly correlated across nearly 800 cancer cell lines.

Cyclin F is a strongly cell cycle-regulated gene. Cyclin F mRNA levels peak in G2/M, and no studies have identified *CCNF* as an E2F target at G1/S. It is therefore unclear how its protein levels increase early in the cell cycle, in lockstep with Skp2, a bona fide E2F target gene. We previously showed that AKT can phosphorylate and stabilize cyclin F, and that this could contribute to its accumulation near G1/S (*Choudhury et al., 2017*). Thus, the activation of cyclin F by AKT could potentially lead to the degradation of p130. Given the recurrent activation of the PI3K-AKT pathway in many cancers, it will be interesting in the future to determine if cyclin F phosphorylation promotes p130 degradation. If true, this would suggest that hyper-activated PI3K, either through mutation of PIK3CA or loss of PTEN, functions through cyclin F to render p130 inactive via the ubiquitin pathway.

Materials and methods
Acquisition and analysis of DEPMAP data
Gene co-dependencies were determined from the Achilles data set from depmap.org (Achilles_gene_effect.csv, downloaded 7/19/19). The Achilles data set contains dependency scores from genome-scale essentiality screens scores of 789 cell lines. As a measure of co-dependency, the Pearson's correlation coefficient of essentiality scores was computed for all gene pairs. GO analysis for the top 100 genes co-dependent with CCNF was performed using MetaScape. Potential cyclin F substrates were identified by proteins encoded by genes that have a Pearson's correlation coefficient of >0.15 when compared to CCNF and are classified by the GO term: cell division (0051301).

Cell lines
Cell lines used include: HEK293T (ATCC), U2OS (ATCC), HeLa (ATCC), HeLa sgCTRL, and HeLa sgCCNF (*Choudhury et al., 2016*), MCF-7 (ATCC), T47D (ATCC), NHF-1 William Kaufman Lab (UNC; retired), IMR-90 (Yue Xiong Lab, UNC; retired), and T98G (Tissue Culture Facility, UNC). Additional cell line details are listed in the table in Appendix 1. Cell line authenticity was verified by SPR. All cell lines were checked for mycoplasma contamination periodically throughout the experimental process.

Cell culture
All cell lines were cultured in Dulbecco's modified Eagle's medium (DMEM; GIBCO) supplemented with 10% fetal bovine serum (FBS; VWR) and 1% Pen/Strep (GIBCO). Cells were incubated at 37°C, 5% CO_2.

DNA transfection experiments were performed in HEK293T cells for 24 hr using either Lipofectamine 2000 (Thermo Fisher Scientific) or PolyJet (SignaGen) transfection reagents according to the manufacturer's protocol. RNA transfection experiments were performed in NHF-1 and IMR-90 cells for 48 hr using RNAiMAX (Thermo Fisher Scientific) transfection reagent according to the manufacturer's protocol. Plasmid and siRNA information is the table in Appendix 1.

To produce lentivirus, HEK293T cells were transfected with pLV[Exp]-CMV> Tet3G/Hygro, pLV[TetOn]-Neo-TRE3G > HA/{p130 WT}, or pLV[TetOn]-Neo-TRE3G > HA/{p130 AA}, and the lentivirus packaging plasmids VSV-G, Gag-pol, Tat, and Rev. Media-containing virus particles were collected after 48 hr, filtered with a 0.45-μM filter, and frozen at –80°C. NHF-1 cells were transduced with a 1:1 ratio of fresh media plus lentivirus-containing media. NHF-1 cells were first transduced with the Tet3G plasmid and selected in media-containing 50 μg/ml hygromycin. Then, NHF-1 cells stably expressing Tet3G were infected with either p130 WT or p130 AA and selected in media-containing 375 μg/ml G418.

Cloning and Directed Mutagenesis pDEST-HA3-p130, pDEST-HA3-p130$^{1–417}$, pDEST-HA3-p130$^{418–1139}$, pDEST-HA3-p130$^{418–616}$, pDEST-HA3-p130$^{418–827}$, pDEST-HA3-p130$^{418–1024}$, pDEST-HA3-p130$^{828–1139}$, and pINDUCER20 CCNF were produced using Gateway Cloning Technology. pLV[Exp]-CMV> Tet3G/Hygro, pLV[TetOn]-Neo-TRE3G > HA/{p130 WT}, or pLV[TetOn]-Neo-TRE3G > HA/{p130 AA} were

all ordered from VectorBuilder. pGEX-GST-p130$^{593–790}$ was a gift from Peter Whyte (McMaster University) and pINDUCER20 was a gift from Stephen Elledge (Addgene #44012). pDEST-HA3-p130 R658A I660A, pDEST-HA3-p130 R680A L682A, and pGEX-GST-p130$^{593–790}$ R680A L682A were generated by site-directed mutagenesis using the Q5 Site-Directed Mutagenesis Kit (NEB) according to the manufacturer's instructions. For recombinant expression, Cyclin F$^{25–546}$ was subcloned into a pFastBac vector with an N-terminal GST tag and TEV protease site. The Skp1 gene (a gift from Dr. Bing Hao) was subcloned into a PGEX-4T-1 vector previously engineered to contain a TEV protease site. Sequences for all primers are included in tables provided in Appendix 1.

Cell lysis and immunoblotting

Cells were lysed on ice for 10 min in NETN (20 mM Tris pH 8.0, 100 mM NaCl, 0.5 mM EDTA, 0.5% NP40) supplemented with 10 µg/ml aprotinin, 10 µg/ml leupeptin, 10 µg/ml pepstatin A, 1 mM sodium orthovanadate, and 1 mM AEBSF(4-[two aminoethyl] benzenesulfonyl fluoride). Following incubation, cells were spun at 20,000×g in a benchtop microcentrifuge at 4°C for 10 min. Protein concentration was determined by Bradford assay (Bio-Rad) and samples were prepared by boiling in Laemmli buffer (LB). Protein was separated by electrophoresis on either homemade or TGX (Bio-Rad) stain-free gels and then was transferred to nitrocellulose membranes. Blocking was performed in 5% non-fat dry milk (Blotting Grade blocker; Bio-Rad) diluted in TBS-T (137 mM NaCl, 2.7 mM KCl, 25 mM Tris pH 7.4, 1 % Tween-20). All primary antibody incubations were carried out overnight, rocking, at 4°C, and all HRP-conjugated antibody incubations were carried out for 1 hr, rocking, at room temperature. TBS-T was used for all wash steps. Protein abundance was visualized by chemiluminescence using Pierce ECL (Thermo Fisher Scientific). A detailed list of antibodies and dilutions is provided in table in Appendix 1.

Immunoprecipitation

Endogenous protein pulldowns:

Asynchronous HEK293T, U2OS, HeLa, or inducible p130 NHF-1 cells were lysed and total protein was quantified as described above. 10% of the protein sample was retained as the input, and the remaining protein was divided in half to be incubated with either rabbit IgG control or Cyclin F antibodies for IP. Cell lysates were incubated for 6 hr, rotating, at 4°C with 1 µg antibody per mg protein. During the incubation, Pierce Protein A/G agarose beads (Thermo Fisher Scientific) were washed 3× for 20 min in NETN, then resuspended at a 50% slurry in NETN. 40 µl slurry per 1 mg protein was added to the protein/antibody IP mix and incubated for 45 min, rotating, at 4°C. Beads were then washed 3× for 5 min in NETN, and finally re-suspended in 2× LB and boiled. Co-IP was assessed by immunoblotting as described.

Exogenous pulldowns:

Asynchronously proliferating inducible p130 NHF-1 cells were treated with 100 ng/ml doxycycline for 24 hr. Cells were lysed and total protein was quantified as above. 10% of the protein sample was retained as the input, and the remaining protein was divided in half to be incubated with either rabbit IgG control or rabbit anti-HA antibodies for IP. IP and washes were carried out as described above. Alternatively, inducible p130 NHF-1 cells were treated with 100 ng/ml doxycycline or water as a vehicle control for 24 hr. Cells were lysed and total protein was quantified as described above. 50 µl of EZView Red anti-HA affinity gel slurry was used to isolate HA-tagged and co-immunoprecipitating proteins. Washes were performed as described above. Co-IP was assessed by immunoblotting.

Protein purification

In order to purify GST and GST-p130 for the in vitro binding assay, BL21 *E. coli* were transformed with GST, GST-p130^{WT} or GST-p130^{AA} and a 0.5-L culture was grown to an O.D. of 0.6 then induced with 1 mM IPTG (Isopropyl β-D-1-thiogalactopyranoside) for 4 hr. Cells were harvested by centrifugation and incubated for 20 min in NTEN *E. coli* Lysis buffer (100 mM NaCl$_2$, 20 mM Tris pH 8.0, 1 mM DTT, 1 mM EDTA, and 1% NP40) supplemented with 10 µg/ml aprotinin, 10 µg/ml leupeptin, 10 µg/ml pepstatin A, and 10 mg/ml lysozyme. Then, cells were lysed by sonication at 50% power for 3× for 30 s pulses, with 1 min on ice between pulses. Lysates were then spun at 30,000×g for 30 min at 4°C to clarify. During the clarification step, glutathione agarose resin (GoldBio) was equilibrated 3× for 10 min in NTEN *E. coli* Lysis buffer. 250 µl of equilibrated glutathione agarose resin was then added to

the clarified lysate and incubated for 2 hr, rotating, at 4°C. Beads were washed 3× for 5 min in NTEN *E. coli* Lysis buffer. Bound GST-p130 was eluted by three sequential elution steps: 2× for 30 min and one overnight incubation, rotating, at 4°C in elution buffer (50 mM Tris pH 8.0, 5 mM reduced glutathione). Elution fractions were pooled, and buffer exchange into 50 mM Tris was performed by 5× buffer exchange in 30,000 MWCO spin columns.

For in vitro ubiquitination assays, UBA1, CDC34B, UBCH7, ARIH1, Cul1-Roc1, and ubiquitin were expressed and purified as described previously (*Kamadurai et al., 2013*; *Scott et al., 2016*). The neddylation of Cul1-Roc1 was also performed as described previously (*Duda et al., 2008*). GST-p130^{wt} (residues 593–790) and GST-p130^{AA} (residues 593–790 R680A L682A) fusions were expressed in *E. coli* BL21-CodonPlus (DE3)-RIL, and then purified by glutathione-affinity and size-exclusion chromatography.

For Cyclin F$^{25-546}$, 1.2 L of Sf9 cells were infected with baculovirus at a density of 2×10^6 cells/ml of culture and harvested after 3 days. Pelleted cells were resuspended in lysis buffer (25 mM Tris, 200 mM NaCl, 1 mM DTT, 1 mM PMSF, 1× protease inhibitor cocktail, pH 8.0) and passed through a C3 emulsiflex homogenizer (AVESTIN, Inc). After lysate clarification, the supernatant was loaded onto a GS4B glutathione agarose (Cytvia) column. The column was washed in lysate buffer lacking protease inhibitors and eluted in the same buffer with 10 mM glutathione. Purified TEV protease (1% by mass) was added overnight while protein was dialyzed in buffer containing 25 mM Tris, 200 mM NaCl, and 1 mM DTT (pH 8.0). Protein was then passed back through a GS4B column to remove free GST, concentrated, and loaded in 1 mL onto a Superdex 200 column (Cytvia) equilibrated in similar buffer. Peak fractions from the column elution were pooled and protein concentrated to 8 μM.

Full-length Skp1 was expressed in *E. coli* as a GST fusion protein. 6 L of BL21(DE3) cells were grown to OD of 0.6 then induced with 1 mM IPTG (Isopropyl β-D-1-thiogalactopyranoside) for 16 hr at room temperature. Protein was purified similar to as described above for cyclin F$^{25–546}$, except that following the initial GS4B elution, protein was further purified by Source Q Sepharose ion-exchange chromatography prior to TEV cleavage. For the fluorescence polarization anisotropy assays, the GST tag was left on the cyclin F for stability, and the fusion protein was mixed with Skp1 prior to the experiment.

P130-cyclin F in vitro binding assays

GST pulldowns were performed by loading 1 μg of purified GST or GST-p130 onto 15 μl of glutathione beads (GoldBio) in NETN (20 mM Tris pH8.0, 100 mM NaCl, 0.5 mM EDTA, 0.5% NP40) for 1 hr, rotating at 4°C. Loaded beads were washed 3× for 5 min in NETN, then incubated with 0.5 mg of whole-cell extract of HEK293T cells transiently transfected with a FLAG-Cyclin F plasmid for 2 hr, rotating, at 4°C. Beads were again washed 3× for 5 min in NETN and p130-cyclin F interaction was assessed by immunoblot.

FLAG pulldowns were performed by immunoprecipitating FLAG-Cyclin F from whole-cell extracts of HEK293T cells transiently transfected with FLAG-Cyclin F. IP was performed by incubating 1 mg whole-cell extract with 50 μl EZView Red anti-FLAG M2 affinity gel (MilliporeSigma) for 2 hr, rotating, at 4°C. Loaded affinity gel was washed 3× for 5 min with NETN, then incubated with 1 μg purified GST or GST-p130 for 2 hr, rotating, at 4°C. Loaded affinity gel was again washed 3× for 5 min in NETN and p130-cyclin F interaction was assessed by immunoblot.

In vitro ubiquitination assay

Multiple turnover reactions were set up by combining 0.1 μM UBA1, 5 mM MgATP, 0.8 μM CDC34B, 0.3 μM ARIH1, 0.8 μM UBCH7, 0.4 μM NEDD8 to Cul1-Roc1,0.4 μM SKP1, 0.4 μM Cyclin F$^{25–546}$, and 0.6 μM of either GST-p130 or GST-p130^{AA} in the assay buffer (20 mM HEPES pH = 8, 200 mM NaCl) while kept on ice. The mixtures were then equilibrated to room temperature and the reaction was started by the addition of 100 μM of ubiquitin. Reactions were quenched by adding SDS loading buffer at specified time points. After SDS-PAGE, the ubiquitination of GST-p130 was monitored by western blot analysis using α-GST antibody (SC-138, mouse) and a fluorescent secondary antibody (goat anti-mouse IgG (H + L), Alexa Fluor 633, A-21052). Fluorescence was observed using the Amersham Typhoon 5.

De-phosphorylation assay with calf intestinal phosphatase

Cells were lysed as described above in NETN lacking EDTA. 20 µg total protein lysates were incubated at 37°C for 1 hr with 1× NEB 2.1 buffer (NEB) with 1 unit of calf intestinal phosphatase (NEB) or buffer as a negative control. As a positive control, 1 mM sodium orthovanadate was added to a reaction containing calf intestinal phosphatase for the duration of the 1-hr incubation. Phosphorylation was assessed by immunoblotting.

Proliferation assays

Cell counting:

NHF-1 inducible p130 cells were seeded in 10 cm plates, and p130 WT or AA was induced by the addition of 100 ng/ml doxycycline (or DMSO as a control) to media. Cells were trypsinized (Gibco), counted with an automatic cell counter (Bio-Rad), and replated in fresh doxycycline-containing media every 48 hr for 2 weeks. Cell count was plotted versus time, differences were assessed using a Student's t-test, and cell count was used to calculate doubling times. Experiments were carried out in triplicate and repeated three times.

PrestoBlue:

NHF-1 inducible p130 cells were seeded in 96-well plates, and p130 WT or AA was induced by the addition of 100 ng/ml doxycycline to media. Media were replaced with fresh doxycycline-containing media every 48 hr for 2 weeks, and growth was assessed with the PrestoBlue cell viability reagent (Thermo Fisher Scientific) on days 1, 7, and 14. Experiments were carried out with six technical replicates, and repeated three times.

Crystal violet assay:

NHF-1 inducible p130 cells were seeded in 60 mm plates, and p130 WT or AA was induced by the addition of 100 ng/ml doxycycline (or DMSO as a control). Media were replaced with fresh doxycycline-containing media (or DMSO-containing media as a control) every 48 hr for 10 days. On day 10, confluence was visualized by staining with Crystal Violet Staining Buffer (0.5% crystal violet, 20% methanol) for 15 min at room temperature, and de-staining with water. Experiments were repeated three times.

RT-qPCR

In NHF-1 inducible p130 cells, p130 WT or AA was induced by the addition of 100 ng/ml doxycycline (or DMSO as a control) for 14 days. Cells were harvested and RNA was extracted using the RNeasy Plus Mini Kit (QIAGEN). 1 µg of extracted RNA was used to generate cDNA libraries using the Super-Script III First-Strand synthesis system (Thermo Fisher Scientific) following the manufacturer's instructions. Samples were diluted 1:10, except for GAPDH analysis that were diluted 1:1000. Transcript abundance was quantified using the SSO Advanced Universal SYBR Green Supermix (Bio-Rad) and measured with a QuantStudio 6 Flex Real-Time PCR System (Thermo Fisher Scientific), and transcript levels were normalized to GAPDH. Relative quantity of transcripts was quantified using the 2-ΔΔCT method. Each sample was run in triplicate. Primers are listed in tables provided in Appendix 1.

Flow cytometry

In NHF-1 inducible p130 cells, p130 WT or AA was induced by the addition of 100 ng/ml doxycycline (or DMSO as a control) for the indicated number of days. For cell cycle analysis: 30 min prior to fixation, cells were pulsed with 10 µM EdU and were fixed in 4% formaldehyde/PBS for 15 min at room temperature. Cells were pelleted and re-suspended in 1% BSA/PBS. EdU was labeled with Alexa Fluor 488 using click chemistry as previously described (*Franks et al., 2020*). For Annexin V apoptosis/necrosis: the dead cell apoptosis kit was used following manufacturer instructions (Thermo Fisher Scientific). Flow was carried out on an Attune NxT Flow Cytometer (Thermo Fisher Scientific), and data were analyzed using FlowJo software.

Florescence polarization anisotropy assay

For the GST-cyclin F$^{25–546}$-Skp1 titration, TAMRA-labeled synthetic peptide (E2F1$^{84–99}$ or p130$^{674–692}$) at 10 nM was mixed with varying concentrations of protein complex in a buffer containing 25 mM Tris,

150 mM NaCl, 1 mM DTT, 0.1% (v/v) Tween-20, pH 8.0. For the K_i measurements, varying concentrations of GST-p130$^{593–790}$ WT, GST-p130$^{593–790}$ R680A/L682A mutant, or synthetic unlabeled E2F1$^{84–99}$ or p130$^{674–692}$ peptide were mixed with 10 nM TAMRA-labeled E2F1$^{84–99}$ and 0.5 µM GST-cyclin F-Skp1 in a buffer containing 25 mM Tris, 150 mM NaCl, 1 mM DTT, 0.1% (v/v) Tween-20, pH 8.0. 40 µl of the reaction were used for the measurement in a 384-well plate. Fluorescence anisotropy (FA) measurements were made in triplicate, using a PerkinElmer EnVision plate reader. The K_D and K_i values were calculated using Prism 8 (Version 8.4.3).

Iterative indirect immunofluorescence imaging (4i)

Cells were plated in glass-bottom plates (Cellvis) treated as required and prepared as follows. In between each step, samples were rinsed 3× with phosphate-buffered saline (PBS) and incubations were at room temperature, unless otherwise stated. Cells were fixed with 4% paraformaldehyde (Thermo Fisher Scientific, 28908) for 30 min, permeabilized with 0.1% Triton X-100 in PBS for 15 min and inspected for sample quality control following Hoechst staining (1:1000, MilliporeSigma, 99403) in imaging buffer (IB: 700 mM N-acetyl-cysteine (Sigma-Aldrich, A7250) in ddH$_2$O. Adjust to pH 7.4). Cells were rinsed 3× with ddH$_2$O and incubated with elution buffer (EB: 0.5 M L-Glycine (Sigma-Aldrich, 50046)), 3 M Urea (Sigma-Aldrich, U4883), 3 M Guanidine chloride (Thermo Fisher Scientific, 15502-016), and 70 mM TCEP-HCl (Sigma-Aldrich, 646547) in ddH$_2$O. Adjusted to (pH 2.5) 3× for 10 min on shaker to remove Hoechst stain. Sample was incubated with 4i blocking solution (sBS: 100 mM maleimide [Sigma-Aldrich, 129585], 100 mM NH$_4$Cl [Sigma-Aldrich, A9434], and 1% bovine serum albumin in PBS) for 1 hr and incubated with primary antibodies diluted as required (anti-phospho-RB [S807/S811] [1:1000, Cell Signaling Technology, 8516]; anti-RB [1:500, Cell Signaling Technology, 9309]; anti-p21 [1:200, R&D Systems, AF1047]; anti-p130 [1:100, Cell Signaling Technology, 13610]; anti-phospho-H2A.X [Ser139] [1:200, Cell Signaling Technology, 80312], anti-phospho-CHK1 [S317] [1:800, Cell Signaling Technology, 12302], anti-53BP1 [1:250, Abcam, ab36823], CDT1 [1:200, Cell Signaling Technology, 8064], CDC6 [1:100, Santa Cruz, sc-9964], HA [1:200, BioLegend, 901501]) in conventional blocking solution (cBS: 1% bovine serum albumin in PBS) overnight at 4°C. Samples were rinsed 3× with PBS and then incubated in secondary antibodies (1:500, donkey anti-rabbit AlexaFluor Plus 488 [Thermo Fisher Scientific, A32790], donkey anti-mouse AlexaFluor Plus 555 [Thermo Fisher Scientific, A32773], and donkey anti-goat AlexaFluor Plus 647 [Thermo Fisher Scientific, A32758]) and Hoechst for 1 hr on shaker, then rinsed 5× with PBS and imaged in IB. Samples were imaged using the Nikon Ti Eclipse inverted microscope with a Nikon Plan Apochromat Lambda 40× objective with a numerical aperture of 0.95 and an Andor Zyla 4.2 sCMOS detector. Stitched 8×8 images were acquired for each condition using the following filter cubes (Chroma): DAPI(383-408/425/435-485nm), GFP(450-490/495/500-550nm), Cy3(530-560/570/573-648nm), and Cy5(590-650/660/663-738nm). After imaging, samples were rinsed 3× with ddH2O, antibodies were eluted, and re-stained iteratively as described above.

4i image analysis

Nuclear segmentation and quantification were performed using standard modules in CellProfiler (v3.1.8) as described below. For each round of immunofluorescence images obtained by 4i, individual nuclei were automatically detected and segmented using the IdentifyPrimaryObjects module. Cytoplasmic segmentation was performed by making a 5-pixel ring outside the nucleus using the ExpandOrShrinkObjects and IdentifyTertiaryObjects modules. Nuclear and cytoplasmic intensities were quantified using the MeasureObjectIntensity module. Distributions of single-cell intensities were visualized using the seaborn library (v0.11.0) in Python (v3.7.1).

Apoptosis assays

Cells were grown for 0–14 days in 100 ng/ml doxycycline or water as a vehicle control. As a positive control for apoptosis. As a positive control, cells were treated with 100 nM staurosporine for 6 hr to induce apoptosis. Presence of cleaved PARP and cleaved Caspase three was assessed by immunoblot. And, apoptosis/necrosis were assessed using an Annexin V/propidium iodide staining kit (Thermo Fisher Scientific) coupled with flow cytometry.

Quantification and statistical analysis

Western blot quantification was carried out using the Fiji software. All statistical analyses were carried out using GraphPad Prism v9.

Acknowledgements

Additional information

Funding

Author contributions

Taylor P Enrico, Conceptualization, Data curation, Formal analysis, Investigation, Methodology, Validation, Visualization, Writing - original draft, Writing – review and editing; Wayne Stallaert, Peter Ngoi, Formal analysis, Investigation, Methodology, Visualization, Writing – review and editing; Elizaveta T Wick, Investigation, Methodology, Writing - original draft, Writing – review and editing; Xianxi Wang, Investigation, Methodology; Seth M Rubin, Nicholas G Brown, Jeremy E Purvis, Conceptualization, Formal analysis, Funding acquisition, Methodology, Project administration, Supervision, Visualization,

Writing – review and editing; Michael J Emanuele, Conceptualization, Funding acquisition, Project administration, Supervision, Visualization, Writing - original draft, Writing – review and editing

Author ORCIDs
Taylor P Enrico http://orcid.org/0000-0002-5453-2868
Seth M Rubin http://orcid.org/0000-0002-1670-4147
Jeremy E Purvis http://orcid.org/0000-0002-6963-0524
Michael J Emanuele http://orcid.org/0000-0003-4104-7449

Decision letter and Author response
Decision letter https://doi.org/10.7554/eLife.70691.sa1
Author response https://doi.org/10.7554/eLife.70691.sa2

Additional files

Supplementary files
• Transparent reporting form

• Source code 1. Violin plotting.

• Source data 1. Immunoblots. This source data file includes all uncropped blots used to generate data for the main figures and figure supplements. Additionally, copies of the uncropped images are shown a second time where blot strips shown in figures are highlighted with a red square and the protein that was blotted for is noted.

• Source data 2. Cycloheximide Chase. This source data file contains quantified band densities and background used to generate the cycloheximide protein degradation plot and for the protein half-life calculations.

• Source data 3. Flow cytometry. This source data file contains percentages of cells in various populations for the flow cytometry experiments.

• Source data 4. Cell counting and PrestoBlue. This source data file contains the raw cell counts for the courting experiment and the raw fluorescence measurements for the PrestoBlue experiment.

• Source data 5. Rt-qPCR. This source data file contains the output from the rt-qPCR machine that was used to determine gene expression for the rt-qPCR blot.

Data availability
Unprocessed, uncropped, immunoblots are made available in the supplemental source data. All raw, unprocessed imaging data is available at Dryad. Raw data related to cell proliferation assays (cell counting and Presto-blue analysis), RT-qPCR, immunoblot quantification for cycloheximide chase experiments and flow cytometry is available in the supplemental source data. All reagents related to this work will be made fully available upon request.

The following dataset was generated:

Author(s)	Year	Dataset title	Dataset URL	Database and Identifier
Enrico T, Stallaert W, Wick E, Ngoi P, Emanuele M, Rubin S, Brown N, Purvis J	2021	Data from: Cyclin F drives proliferation through SCF-dependent degradation of the retinoblastoma-like tumor suppressor p130/RBL2	https://doi.org/10.5061/dryad.69p8cz93d	Dryad Digital Repository, 10.5061/dryad.69p8cz93d

The following previously published datasets were used:

References

Agostinetto E, Vian L, Caparica R, Bruzzone M, Ceppi M, Lambertini M, Pondé N, de Azambuja E. 2021. CDK4/6 inhibitors as adjuvant treatment for hormone receptor-positive, HER2-negative early breast cancer: a systematic review and meta-analysis. *ESMO Open* 6:100091. DOI: https://doi.org/10.1016/j.esmoop.2021.100091, PMID: 33743330

Bai C, Richman R, Elledge SJ. 1994. Human cyclin F. *The EMBO Journal* 13:6087–6098. DOI: https://doi.org/10.1002/j.1460-2075.1994.tb06955.x, PMID: 7813445

Bai C, Sen P, Hofmann K, Ma L, Goebl M, Harper JW, Elledge SJ. 1996. SKP1 connects cell cycle regulators to the ubiquitin proteolysis machinery through a novel motif, the F-box. *Cell* **86**:263–274. DOI: https://doi.org/10.1016/s0092-8674(00)80098-7, PMID: 8706131

Baldi A, Esposito V. 1997. Differential Tissues and Expression in Primary Lung and in Normal Human Tissues and in Primary Lung Cancer. *Clinical Cancer Research* **3**:1691–1697.

Bassermann F, Eichner R, Pagano M. 2014. The ubiquitin proteasome system - implications for cell cycle control and the targeted treatment of cancer. *Biochimica et Biophysica Acta* **1843**:150–162. DOI: https://doi.org/10.1016/j.bbamcr.2013.02.028, PMID: 23466868

Bellan C, De Falco G, Tosi GM, Lazzi S, Ferrari F, Morbini G, Bartolomei S, Toti P, Mangiavacchi P, Cevenini G, Trimarchi C, Cinti C, Giordano A, Leoncini L, Tosi P, Cottier H. 2002. Missing expression of pRb2/p130 in human retinoblastomas is associated with reduced apoptosis and lesser differentiation. *Investig Ophthalmol Vis Sci* **43**:3602–3608.

Bhattacharya S, Garriga J, Calbó J, Yong T, Haines DS, Graña X. 2003. SKP2 associates with p130 and accelerates p130 ubiquitylation and degradation in human cells. *Oncogene* **22**:2443–2451. DOI: https://doi.org/10.1038/sj.onc.1206339, PMID: 12717421

Boyle EA, Pritchard JK, Greenleaf WJ. 2018. High-resolution mapping of cancer cell networks using co-functional interactions. *Molecular Systems Biology* **14**:8594. DOI: https://doi.org/10.15252/msb.20188594, PMID: 30573688

Burdova K, Yang H, Faedda R, Hume S, Chauhan J, Ebner D, Kessler BM, Vendrell I, Drewry DH, Wells CI, Hatch SB, Dianov GL, Buffa FM, D'Angiolella V. 2019. E2F1 proteolysis via SCF-cyclin F underlies synthetic lethality between cyclin F loss and Chk1 inhibition. *The EMBO Journal* **38**:e101443. DOI: https://doi.org/10.15252/embj.2018101443, PMID: 31424118

Canhoto AJ, Chestukhin A, Litovchick L, DeCaprio JA. 2000. Phosphorylation of the retinoblastoma-related protein p130 in growth-arrested cells. *Oncogene* **19**:5116–5122. DOI: https://doi.org/10.1038/sj.onc.1203893, PMID: 11042701

Cardozo T, Pagano M. 2004. The SCF ubiquitin ligase: insights into a molecular machine. *Nature Reviews. Molecular Cell Biology* **5**:739–751. DOI: https://doi.org/10.1038/nrm1471, PMID: 15340381

Carrano AC, Eytan E, Hershko A, Pagano M. 1999. SKP2 is required for ubiquitin-mediated degradation of the CDK inhibitor p27. *Nature Cell Biology* **1**:193–199. DOI: https://doi.org/10.1038/12013, PMID: 10559916

Castaño E, Kleyner Y, Dynlacht BD. 1998. Dual cyclin-binding domains are required for p107 to function as a kinase inhibitor. *Molecular and Cellular Biology* **18**:5380–5391. DOI: https://doi.org/10.1128/MCB.18.9.5380, PMID: 9710622

Choudhury R, Bonacci T, Arceci A, Lahiri D, Mills CA, Kernan JL, Branigan TB, DeCaprio JA, Burke DJ, Emanuele MJ. 2016. APC/C and SCF cyclin F Constitute a Reciprocal Feedback Circuit Controlling S-Phase Entry. *Cell Reports* **16**:3359–3372. DOI: https://doi.org/10.1016/j.celrep.2016.08.058

Choudhury R, Bonacci T, Wang X, Truong A, Arceci A, Zhang Y, Mills CA, Kernan JL, Liu P, Emanuele MJ. 2017. The E3 Ubiquitin Ligase SCF(Cyclin F) Transmits AKT Signaling to the Cell-Cycle Machinery. *Cell Reports* **20**:3212–3222. DOI: https://doi.org/10.1016/j.celrep.2017.08.099, PMID: 28954236

Claudio PP, Howard CM, Baldi A, De Luca A, Fu Y, Condorelli G, Sun Y, Colburn N, Calabretta B, Giordano A. 1994. p130/pRb2 has growth suppressive properties similar to yet distinctive from those of retinoblastoma family members pRb and p107. *Cancer Research* **54**:5556–5560 PMID: 7923196.,

Clijsters L, Hoencamp C, Calis JJA, Marzio A, Handgraaf SM, Cuitino MC, Rosenberg BR, Leone G, Pagano M. 2019. Cyclin F Controls Cell-Cycle Transcriptional Outputs by Directing the Degradation of the Three Activator E2Fs. *Molecular Cell* **74**:1264-1277.. DOI: https://doi.org/10.1016/j.molcel.2019.04.010, PMID: 31130363

Dankert JF, Rona G, Clijsters L, Geter P, Skaar JR, Bermudez-Hernandez K, Sassani E, Fenyö D, Ueberheide B, Schneider R, Pagano M. 2016. Cyclin F-Mediated Degradation of SLBP Limits H2A.X Accumulation and Apoptosis upon Genotoxic Stress in G2. *Molecular Cell* **64**:507–519. DOI: https://doi.org/10.1016/j.molcel.2016.09.010, PMID: 27773672

Dannenberg J-H, Schuijff L, Dekker M, van der Valk M, te Riele H. 2004. Tissue-specific tumor suppressor activity of retinoblastoma gene homologs p107 and p130. *Genes & Development* **18**:2952–2962. DOI: https://doi.org/10.1101/gad.322004, PMID: 15574596

Dempster JM, Pacini C, Pantel S, Behan FM, Green T, Krill-Burger J, Beaver CM, Younger ST, Zhivich V, Najgebauer H, Allen F, Gonçalves E, Shepherd R, Doench JG, Yusa K, Vazquez F, Parts L, Boehm JS, Golub TR, Hahn WC, et al. 2019. Agreement between two large pan-cancer CRISPR-Cas9 gene dependency data sets. *Nature Communications* **10**:5817. DOI: https://doi.org/10.1038/s41467-019-13805-y, PMID: 31862961

Doench JG, Fusi N, Sullender M, Hegde M, Vaimberg EW, Donovan KF, Smith I, Tothova Z, Wilen C, Orchard R, Virgin HW, Listgarten J, Root DE. 2016. Optimized sgRNA design to maximize activity and minimize off-target effects of CRISPR-Cas9. *Nature Biotechnology* **34**:184–191. DOI: https://doi.org/10.1038/nbt.3437, PMID: 26780180

Duda DM, Borg LA, Scott DC, Hunt HW, Hammel M, Schulman BA. 2008. Structural insights into NEDD8 activation of cullin-RING ligases: conformational control of conjugation. *Cell* **134**:995–1006. DOI: https://doi.org/10.1016/j.cell.2008.07.022, PMID: 18805092

Dyson N. 1998. The regulation of E2F by pRB-family proteins. *Genes & Development* **12**:2245–2262. DOI: https://doi.org/10.1101/gad.12.15.2245, PMID: 9694791

Dyson NJ. 2016. RB1: a prototype tumor suppressor and an enigma. *Genes & Development* **30**:1492–1502. DOI: https://doi.org/10.1101/gad.282145.116, PMID: 27401552

D'Angiolella V, Donato V, Vijayakumar S, Saraf A, Florens L, Washburn MP, Dynlacht B, Pagano M. 2010. SCF(Cyclin F) controls centrosome homeostasis and mitotic fidelity through CP110 degradation. *Nature* **466**:138–142. DOI: https://doi.org/10.1038/nature09140, PMID: 20596027

D'Angiolella V, Donato V, Forrester FM, Jeong Y-T, Pellacani C, Kudo Y, Saraf A, Florens L, Washburn MP, Pagano M. 2012. Cyclin F-mediated degradation of ribonucleotide reductase M2 controls genome integrity and DNA repair. *Cell* **149**:1023–1034. DOI: https://doi.org/10.1016/j.cell.2012.03.043, PMID: 22632967

D'Angiolella V, Esencay M, Pagano M. 2013. A cyclin without cyclin-dependent kinases: cyclin F controls genome stability through ubiquitin-mediated proteolysis. *Trends in Cell Biology* **23**:135–140. DOI: https://doi.org/10.1016/j.tcb.2012.10.011, PMID: 23182110

Emanuele MJ, Enrico TP, Mouery RD, Wasserman D, Nachum S, Tzur A. 2020. Complex Cartography: Regulation of E2F Transcription Factors by Cyclin F and Ubiquitin. *Trends in Cell Biology* **30**:640–652. DOI: https://doi.org/10.1016/j.tcb.2020.05.002, PMID: 32513610

Engeland K. 2018. Cell cycle arrest through indirect transcriptional repression by p53: I have a DREAM. *Cell Death and Differentiation* **25**:114–132. DOI: https://doi.org/10.1038/cdd.2017.172, PMID: 29125603

Farkas T, Hansen K, Holm K, Lukas J, Bartek J. 2002. Distinct phosphorylation events regulate p130- and p107-mediated repression of E2F-4. *The Journal of Biological Chemistry* **277**:26741–26752. DOI: https://doi.org/10.1074/jbc.M200381200, PMID: 12006580

Feldman RMR, Correll CC, Kaplan KB, Deshaies RJ. 1997. A complex of Cdc4p, Skp1p, and Cdc53p/cullin catalyzes ubiquitination of the phosphorylated CDK inhibitor Sic1p. *Cell* **91**:221–230. DOI: https://doi.org/10.1016/s0092-8674(00)80404-3, PMID: 9346239

Fischer M, Grossmann P, Padi M, DeCaprio JA. 2016. Integration of TP53, DREAM, MMB-FOXM1 and RB-E2F target gene analyses identifies cell cycle gene regulatory networks. *Nucleic Acids Research* **44**:6070–6086. DOI: https://doi.org/10.1093/nar/gkw523, PMID: 27280975

Forristal C, Henley SA, MacDonald JI, Bush JR, Ort C, Passos DT, Talluri S, Ishak CA, Thwaites MJ, Norley CJ, Litovchick L, DeCaprio JA, DiMattia G, Holdsworth DW, Beier F, Dick FA. 2014. Loss of the mammalian DREAM complex deregulates chondrocyte proliferation. *Molecular and Cellular Biology* **34**:2221–2234. DOI: https://doi.org/10.1128/MCB.01523-13, PMID: 24710275

Franks JL, Martinez-Chacin RC, Wang X, Tiedemann RL, Bonacci T, Choudhury R, Bolhuis DL, Enrico TP, Mouery RD, Damrauer JS, Yan F, Harrison JS, Major MB, Hoadley KA, Suzuki A, Rothbart SB, Brown NG, Emanuele MJ. 2020. In silico APC/C substrate discovery reveals cell cycle-dependent degradation of UHRF1 and other chromatin regulators. *PLOS Biology* **18**:e3000975. DOI: https://doi.org/10.1371/journal.pbio.3000975, PMID: 33306668

Fry DW, Harvey PJ, Keller PR, Elliott WL, Meade M, Trachet E, Albassam M, Zheng X, Leopold WR, Pryer NK, Toogood PL. 2004. Specific inhibition of cyclin-dependent kinase 4/6 by PD 0332991 and associated antitumor activity in human tumor xenografts. *Molecular Cancer Therapeutics* **3**:1427–1438 PMID: 15542782.,

Gut G, Herrmann MD, Pelkmans L. 2018. Multiplexed protein maps link subcellular organization to cellular states. *Science* **361**:eaar7042. DOI: https://doi.org/10.1126/science.aar7042, PMID: 30072512

Hansen K, Farkas T, Lukas J, Holm K, Rönnstrand L, Bartek J. 2001. Phosphorylation-dependent and -independent functions of p130 cooperate to evoke a sustained G1 block. *The EMBO Journal* **20**:422–432. DOI: https://doi.org/10.1093/emboj/20.3.422, PMID: 11157749

Horn-Ghetko D, Krist DT, Prabu JR, Baek K, Mulder MPC, Klügel M, Scott DC, Ovaa H, Kleiger G, Schulman BA. 2021. Ubiquitin ligation to F-box protein targets by SCF-RBR E3-E3 super-assembly. *Nature* **590**:671–676. DOI: https://doi.org/10.1038/s41586-021-03197-9, PMID: 33536622

Iness AN, Felthousen J, Ananthapadmanabhan V, Sesay F, Saini S, Guiley KZ, Rubin SM, Dozmorov M, Litovchick L. 2019. The cell cycle regulatory DREAM complex is disrupted by high expression of oncogenic B-Myb. *Oncogene* **38**:1080–1092. DOI: https://doi.org/10.1038/s41388-018-0490-y, PMID: 30206359

Ito Y, Yoshida H, Uruno T, Nakano K, Takamura Y, Miya A, Kobayashi K, Yokozawa T, Matsuzuka F, Kuma K, Miyauchi A. 2003. p130 expression in thyroid neoplasms: its linkage with tumor size and dedifferentiation. *Cancer Letters* **192**:83–87. DOI: https://doi.org/10.1016/s0304-3835(02)00627-4, PMID: 12637156

Kamadurai HB, Qiu Y, Deng A, Harrison JS, Macdonald C, Actis M, Rodrigues P, Miller DJ, Souphron J, Lewis SM, Kurinov I, Fujii N, Hammel M, Piper R, Kuhlman B, Schulman BA. 2013. Mechanism of ubiquitin ligation and lysine prioritization by a HECT E3. *eLife* **2**:e00828. DOI: https://doi.org/10.7554/eLife.00828, PMID: 23936628

Kay C, Martínez-Pérez C, Meehan J, Gray M, Webber V, Dixon JM, Turnbull AK. 2021. Current trends in the treatment of HR+/HER2+ breast cancer. *Future Oncology* **17**:1665–1681. DOI: https://doi.org/10.2217/fon-2020-0504, PMID: 33726508

Klein DK, Hoffmann S, Ahlskog JK, O'Hanlon K, Quaas M, Larsen BD, Rolland B, Rösner HI, Walter D, Kousholt AN, Menzel T, Lees M, Johansen JV, Rappsilber J, Engeland K, Sørensen CS. 2015. Cyclin F suppresses B-Myb activity to promote cell cycle checkpoint control. *Nature Communications* **6**:5800. DOI: https://doi.org/10.1038/ncomms6800, PMID: 25557911

Kory N, Uit de Bos J, van der Rijt S, Jankovic N, Güra M, Arp N, Pena IA, Prakash G, Chan SH, Kunchok T, Lewis CA, Sabatini DM. 2020. MCART1/SLC25A51 is required for mitochondrial NAD transport. *Science Advances* **6**:eabe5310. DOI: https://doi.org/10.1126/sciadv.abe5310, PMID: 33087354

Lacy S, Whyte P. 1997. Identification of a p130 domain mediating interactions with cyclin A/cdk 2 and cyclin E/cdk 2 complexes. *Oncogene* **14**:2395–2406. DOI: https://doi.org/10.1038/sj.onc.1201085, PMID: 9188854

Litovchick L, Sadasivam S, Florens L, Zhu X, Swanson SK, Velmurugan S, Chen R, Washburn MP, Liu XS, DeCaprio JA. 2007. Evolutionarily conserved multisubunit RBL2/p130 and E2F4 protein complex represses

human cell cycle-dependent genes in quiescence. *Molecular Cell* **26**:539–551. DOI: https://doi.org/10.1016/j.molcel.2007.04.015, PMID: 17531812

Liu H, Wang J, Liu Y, Hu L, Zhang C, Xing B, Du X. 2018. Human U3 protein14a is a novel type ubiquitin ligase that binds RB and promotes RB degradation depending on a leucine-rich region. *Biochimica et Biophysica Acta. Molecular Cell Research* **1865**:1611–1620. DOI: https://doi.org/10.1016/j.bbamcr.2018.08.016, PMID: 30327202

Lukas J, Herzinger T, Hansen K, Moroni MC, Resnitzky D, Helin K, Reed SI, Bartek J. 1997. Cyclin E-induced S phase without activation of the pRb/E2F pathway. *Genes & Development* **11**:1479–1492. DOI: https://doi.org/10.1101/gad.11.11.1479, PMID: 9192874

Mavrommati I, Faedda R, Galasso G, Li J, Burdova K, Fischer R, Kessler BM, Carrero ZI, Guardavaccaro D, Pagano M, D'Angiolella V. 2018. β-TrCP- and Casein Kinase II-Mediated Degradation of Cyclin F Controls Timely Mitotic Progression. *Cell Reports* **24**:3404–3412. DOI: https://doi.org/10.1016/j.celrep.2018.08.076, PMID: 30257202

McDonald ER, de Weck A, Schlabach MR, Billy E, Mavrakis KJ, Hoffman GR, Belur D, Castelletti D, Frias E, Gampa K, Golji J, Kao I, Li L, Megel P, Perkins TA, Ramadan N, Ruddy DA, Silver SJ, Sovath S, Stump M, et al. 2017. Project DRIVE: A Compendium of Cancer Dependencies and Synthetic Lethal Relationships Uncovered by Large-Scale, Deep RNAi Screening. *Cell* **170**:577–592. DOI: https://doi.org/10.1016/j.cell.2017.07.005, PMID: 28753431

Müller GA, Quaas M, Schümann M, Krause E, Padi M, Fischer M, Litovchick L, DeCaprio JA, Engeland K. 2012. The CHR promoter element controls cell cycle-dependent gene transcription and binds the DREAM and MMB complexes. *Nucleic Acids Research* **40**:1561–1578. DOI: https://doi.org/10.1093/nar/gkr793, PMID: 22064854

Munoz DM, Cassiani PJ, Li L, Billy E, Korn JM, Jones MD, Golji J, Ruddy DA, Yu K, McAllister G, DeWeck A, Abramowski D, Wan J, Shirley MD, Neshat SY, Rakiec D, de Beaumont R, Weber O, Kauffmann A, McDonald ER, et al. 2016. CRISPR Screens Provide a Comprehensive Assessment of Cancer Vulnerabilities but Generate False-Positive Hits for Highly Amplified Genomic Regions. *Cancer Discovery* **6**:900–913. DOI: https://doi.org/10.1158/2159-8290.CD-16-0178, PMID: 27260157

Narasimha AM, Kaulich M, Shapiro GS, Choi YJ, Sicinski P, Dowdy SF. 2014. Cyclin D activates the Rb tumor suppressor by mono-phosphorylation. *eLife* **3**:e02872. DOI: https://doi.org/10.7554/eLife.02872

Ng SR, Rideout WM, Akama-Garren EH, Bhutkar A, Mercer KL, Schenkel JM, Bronson RT, Jacks T. 2020. CRISPR-mediated modeling and functional validation of candidate tumor suppressor genes in small cell lung cancer. *PNAS* **117**:513–521. DOI: https://doi.org/10.1073/pnas.1821893117, PMID: 31871154

Ohh M, Kim WY, Moslehi JJ, Chen Y, Chau V, Read MA, Kaelin WG. 2002. An intact NEDD8 pathway is required for Cullin-dependent ubiquitylation in mammalian cells. *EMBO Reports* **3**:177–182. DOI: https://doi.org/10.1093/embo-reports/kvf028, PMID: 11818338

Pan J, Meyers RM, Michel BC, Mashtalir N, Sizemore AE, Wells JN, Cassel SH, Vazquez F, Weir BA, Hahn WC, Marsh JA, Tsherniak A, Kadoch C. 2018. Interrogation of Mammalian Protein Complex Structure, Function, and Membership Using Genome-Scale Fitness Screens. *Cell Systems* **6**:555-568.. DOI: https://doi.org/10.1016/j.cels.2018.04.011, PMID: 29778836

Patel AJ, Wan YW, Al-Ouran R, Revelli JP, Cardenas MF, Oneissi M, Xi L, Jalali A, Magnotti JF, Muzny DM, Doddapaneni H, Sebastian S, Heck KA, Goodman JC, Gopinath SP, Liu Z, Rao G, Plon SE, Yoshor D, Wheeler DA, et al. 2019. Molecular profiling predicts meningioma recurrence and reveals loss of DREAM complex repression in aggressive tumors. *PNAS* **116**:21715–21726. DOI: https://doi.org/10.1073/pnas.1912858116, PMID: 31591222

Pentimalli F, Forte IM, Esposito L, Indovina P, Iannuzzi CA, Alfano L, Costa C, Barone D, Rocco G, Giordano A. 2018. RBL2/p130 is a direct AKT target and is required to induce apoptosis upon AKT inhibition in lung cancer and mesothelioma cell lines. *Oncogene* **37**:3657–3671. DOI: https://doi.org/10.1038/s41388-018-0214-3, PMID: 29606701

Rubin SM, Sage J, Skotheim JM. 2020. Integrating Old and New Paradigms of G1/S Control. *Molecular Cell* **80**:183–192. DOI: https://doi.org/10.1016/j.molcel.2020.08.020, PMID: 32946743

Sadasivam S, DeCaprio JA. 2013. The DREAM complex: master coordinator of cell cycle-dependent gene expression. *Nature Reviews. Cancer* **13**:585–595. DOI: https://doi.org/10.1038/nrc3556, PMID: 23842645

Schade AE, Fischer M, DeCaprio JA. 2019. RB, p130 and p107 differentially repress G1/S and G2/M genes after p53 activation. *Nucleic Acids Research* **47**:11197–11208. DOI: https://doi.org/10.1093/nar/gkz961, PMID: 31667499

Schade AE, Oser MG, Nicholson HE, DeCaprio JA. 2020. Cyclin D-CDK4 relieves cooperative repression of proliferation and cell cycle gene expression by DREAM and RB. *Oncogene* **38**:4962–4976. DOI: https://doi.org/10.1038/s41388-019-0767-9, PMID: 30833638

Schaffer BE, Park KS, Yiu G, Conklin JF, Lin C, Burkhart DL, Karnezis AN, Sweet-Cordero EA, Sage J. 2010. Loss of p130 accelerates tumor development in a mouse model for human small-cell lung carcinoma. *Cancer Research* **70**:3877–3883. DOI: https://doi.org/10.1158/0008-5472.CAN-09-4228, PMID: 20406986

Schmoller KM, Turner JJ, Kõivomägi M, Skotheim JM. 2015. Dilution of the cell cycle inhibitor Whi5 controls budding-yeast cell size. *Nature* **526**:268–272. DOI: https://doi.org/10.1038/nature14908, PMID: 26390151

Schwob E, Böhm T, Mendenhall MD, Nasmyth K. 1994. The B-type cyclin kinase inhibitor p40SIC1 controls the G1 to S transition in *S. cerevisiae*. *Cell* **79**:233–244. DOI: https://doi.org/10.1016/0092-8674(94)90193-7, PMID: 7954792

Scott DC, Rhee DY, Duda DM, Kelsall IR, Olszewski JL, Paulo JA, de Jong A, Ovaa H, Alpi AF, Harper JW, Schulman BA. 2016. Two Distinct Types of E3 Ligases Work in Unison to Regulate Substrate Ubiquitylation. *Cell* **166**:1198-1214.. DOI: https://doi.org/10.1016/j.cell.2016.07.027, PMID: 27565346

Skowyra D, Craig KL, Tyers M, Elledge SJ, Harper JW. 1997. F-box proteins are receptors that recruit phosphorylated substrates to the SCF ubiquitin-ligase complex. *Cell* **91**:209–219. DOI: https://doi.org/10.1016/s0092-8674(00)80403-1, PMID: 9346238

Smith EJ, Leone G, DeGregori J, Jakoi L, Nevins JR. 1996. The accumulation of an E2F-p130 transcriptional repressor distinguishes a G0 cell state from a G1 cell state. *Molecular and Cellular Biology* **16**:6965–6976. DOI: https://doi.org/10.1128/MCB.16.12.6965, PMID: 8943352

Soucy TA, Smith PG, Milhollen MA, Berger AJ, Gavin JM, Adhikari S, Brownell JE, Burke KE, Cardin DP, Critchley S, Cullis CA, Doucette A, Garnsey JJ, Gaulin JL, Gershman RE, Lublinsky AR, McDonald A, Mizutani H, Narayanan U, Olhava EJ, et al. 2009. An inhibitor of NEDD8-activating enzyme as a new approach to treat cancer. *Nature* **458**:732–736. DOI: https://doi.org/10.1038/nature07884, PMID: 19360080

Susini T, Baldi F, Howard CM, Baldi A, Taddei G, Massi D, Rapi S, Savino L, Massi G, Giordano A. 1998. Expression of the retinoblastoma-related gene Rb2/p130 correlates with clinical outcome in endometrial cancer. *Journal of Clinical Oncology* **16**:1085–1093. DOI: https://doi.org/10.1200/JCO.1998.16.3.1085, PMID: 9508194

Tanaka N, Ogi K, Odajima T, Dehari H, Yamada S, Sonoda T, Kohama G. 2001. pRb2/p130 protein expression is correlated with clinicopathologic findings in patients with oral squamous cell carcinoma. *Cancer* **92**:2117–2125. DOI: https://doi.org/10.1002/1097-0142(20011015)92:8<2117::aid-cncr1553>3.0.co;2-o, PMID: 11596028

Tedesco D, Lukas J, Reed SI. 2002. The pRb-related protein p130 is regulated by phosphorylation-dependent proteolysis via the protein-ubiquitin ligase SCF(Skp2). *Genes & Development* **16**:2946–2957. DOI: https://doi.org/10.1101/gad.1011202, PMID: 12435635

Topacio BR, Zatulovskiy E, Cristea S, Xie S, Tambo CS, Rubin SM, Sage J, Kõivomägi M, Skotheim JM. 2019. Cyclin D-Cdk4,6 Drives Cell-Cycle Progression via the Retinoblastoma Protein's C-Terminal Helix. *Molecular Cell* **74**:758-770.. DOI: https://doi.org/10.1016/j.molcel.2019.03.020, PMID: 30982746

Ventura E, Pentimalli F, Giordano A. 2018. RBL2/p130: a direct AKT substrate and mediator of AKT inhibition-induced apoptosis. *Oncoscience* **5**:278–280. DOI: https://doi.org/10.18632/oncoscience.467, PMID: 30652113

Wang Y, Zheng Z, Zhang J, Wang Y, Kong R, Liu J, Zhang Y, Deng H, Du X, Ke Y. 2015. A Novel Retinoblastoma Protein (RB) E3 Ubiquitin Ligase (NRBE3) Promotes RB Degradation and Is Transcriptionally Regulated by E2F1 Transcription Factor. *The Journal of Biological Chemistry* **290**:28200–28213. DOI: https://doi.org/10.1074/jbc.M115.655597, PMID: 26442585

Wang T, Yu H, Hughes NW, Liu B, Kendirli A, Klein K, Chen WW, Lander ES, Sabatini DM. 2017. Gene Essentiality Profiling Reveals Gene Networks and Synthetic Lethal Interactions with Oncogenic Ras. *Cell* **168**:890-903.. DOI: https://doi.org/10.1016/j.cell.2017.01.013, PMID: 28162770

Wasserman D, Nachum S, Cohen M, Enrico TP, Noach-Hirsh M, Parasol J, Zomer-Polak S, Auerbach N, Sheinberger-Chorni E, Nevenzal H, Levi-Dadon N, Wang X, Lahmi R, Michaely E, Gerber D, Emanuele MJ, Tzur A. 2020. Cell cycle oscillators underlying orderly proteolysis of E2F8. *Molecular Biology of the Cell* **31**:725–740. DOI: https://doi.org/10.1091/mbc.E19-12-0725, PMID: 31995441

White EA, Sowa ME, Tan MJA, Jeudy S, Hayes SD, Santha S, Münger K, Harper JW, Howley PM. 2012. Systematic identification of interactions between host cell proteins and E7 oncoproteins from diverse human papillomaviruses. *PNAS* **109**:E260–E267. DOI: https://doi.org/10.1073/pnas.1116776109, PMID: 22232672

Yuan R, Liu Q, Segeren HA, Yuniati L, Guardavaccaro D, Lebbink RJ, Westendorp B, de Bruin A. 2019. Cyclin F-dependent degradation of E2F7 is critical for DNA repair and G2-phase progression. *The EMBO Journal* **38**:e101430. DOI: https://doi.org/10.15252/embj.2018101430, PMID: 31475738

Zamparelli A, Masciullo V, Bovicelli A, Santini D, Ferrandina G, Minimo C, Terzano P, Costa S, Cinti C, Ceccarelli C, Mancuso S, Scambia G, Bovicelli L, Giordano A. 2001. Expression of cell-cycle-associated proteins pRB2/p130 and p27kip in vulvar squamous cell carcinomas. *Human Pathology* **32**:4–9. DOI: https://doi.org/10.1053/hupa.2001.20371, PMID: 11172288

Zatulovskiy E, Zhang S, Berenson DF, Topacio BR, Skotheim JM. 2020. Cell growth dilutes the cell cycle inhibitor Rb to trigger cell division. *Science* **369**:466–471. DOI: https://doi.org/10.1126/science.aaz6213, PMID: 32703881

Zhu L, van den Heuvel S, Helin K, Fattaey A, Ewen M, Livingston D, Dyson N, Harlow E. 1993. Inhibition of cell proliferation by p107, a relative of the retinoblastoma protein. *Genes & Development* **7**:1111–1125. DOI: https://doi.org/10.1101/gad.7.7a.1111, PMID: 8319904

Appendix 1

Key reagents table
Lists key reagents used in this study.

Appendix 1—key resources table

Reagent type (species) or resource	Designation	Source or reference	Identifiers	Additional information
Gene (*Homo sapiens*)	CCNF	GenBank	Gene ID: 899	
Gene (*H. sapiens*)	RBL2	GenBank	Gene ID: 5934	
Antibody	CDK4 (rabbit monoclonal) antibody	CST	Cat. #: D9GE3; RRID:AB_2799229	IB (1:1000)
Antibody	CDK6 (rabbit monoclonal) antibody	CST	Cat. #:D4S8S; RRID:AB_2721897	IB (1:1000)
Antibody	Cyclin A1 (rabbit monoclonal) antibody	Abcam	Cat. #: ab53699; RRID:AB_879763	IB (1:1000)
Antibody	Cyclin A1 (mouse monoclonal) antibody	Santa Cruz	Cat. #: SC-751; RRID:AB_631329	IB (1:5000); IP (1 µg)
Antibody	Cyclin D1 (rabbit monoclonal) antibody	CST	Cat. #: 2978; RRID:AB_2259616	IB (1:1000)
Antibody	Cyclin E1 (mouse monoclonal) antibody	CST	Cat. #: 4129; RRID:AB_2071200	IB (1:5000); IP (1 µg)
Antibody	Cyclin E1 (rabbit monoclonal) antibody	CST	Cat. #: 20808; RRID:AB_2783554	IB (1:1000)
Antibody	Cyclin F (rabbit polyclonal) antibody	Santa Cruz	Cat. #: SC-952; RRID:AB_2071212	IB (1:5000)
Antibody	FLAG (HRP-conjugated mouse monoclonal) antibody	Sigma-Aldrich	Cat. #: A8592; RRID:AB_439702	IB (1:10,000)
Antibody	GAPDH (mouse monoclonal) antibody	Santa Cruz	Cat. #: sc-47724; RRID:AB_627678	IB (1:5000)
Antibody	GST (HRP-conjugated mouse monoclonal) antibody	GeneTex	Cat. #: GTX114099; RRID:AB_1949436	IB (1:5000)
Antibody	HA (mouse monoclonal) antibody	Covance/ BioLegend	Covance Cat. #: MMS-101P; RRID:AB_2314672	IB (1:2000)
Antibody	Lin54 (rabbit polyclonal) antibody	Bethyl	Cat. #: A303-799A; RRID:AB_11218173	IB (1:1000)
Antibody	Normal rabbit IgG (polyclonal) antibody	ProteinTech	Cat. #: 30000-0-AP; RRID:AB_2819035	IP (1 µg)
Antibody	p107 (rabbit monoclonal) antibody	CST	Cat. #: D3P3C; RRID:AB_2800144	IB (1:1000)
Antibody	p130 (rabbit monoclonal) antibody	CST	Cat. #: D9T7M; RRID:AB_2798274	IB (1:1000)
Antibody	p130 pS672 (rabbit monoclonal) antibody	Abcam	Cat. #: ab76255; RRID:AB_2284799	IB (1:5000)
Antibody	p27 (rabbit monoclonal) antibody	CST	Cat. #: 2552; RRID:AB_10693314	IB (1:1000)
Antibody	Skp2 (rabbit monoclonal) antibody	CST	Cat. #: 2652; RRID:AB_11178941	IB (1:5000)
Antibody	Tubulin (mouse monoclonal) antibody	Santa Cruz	Cat. #: 32293; RRID:AB_628412	IB (1:5000)

Appendix 1 Continued on next page

Appendix 1 Continued

Reagent type (species) or resource	Designation	Source or reference	Identifiers	Additional information
Antibody	Goat anti-mouse IgG HRP-conjugated (goat polyclonal) antibody	Jackson ImmunoResearch	Cat. #: 115-035-003; RRID:AB_10015289	IB (1:5000)
Antibody	Goat anti-rabbit IgG HRP-conjugated (goat polyclonal) antibody	Jackson ImmunoResearch	Cat. #: 111-035-003; RRID:AB_2313567	IB (1:5000)
Antibody	Phospho-RB(S807/S811) (rabbit monoclonal) antibody	CST	Cat. #: 8516; RRID:AB_11178658	4i (1:1000)
Antibody	RB (mouse monoclonal) antibody	CST	Cat. #: 9309; RRID:AB_823629	4i (1:500)
Antibody	p21 (goat polyclonal) antibody	R&D Systems	Cat. #: AF1047; RRID:AB_2244704	4i (1:200)
Antibody	p130 (rabbit monoclonal) antibody	CST	Cat. #: 13610; RRID:AB_2798274	4i (1:100)
Antibody	Phospho-H2A.X(ser139) (mouse monoclonal) antibody	CST	Cat. #: 80312; RRID:AB_2799949	4i (1:200)
Antibody	Anti-phospho-Chk1 (rabbit monoclonal) antibody	CST	Cat. #: 12302; RRID:AB_2783865	4i (1:800)
Antibody	53 BP1 (rabbit polyclonal) antibody	Abcam	Cat. #: ab36823; RRID:AB_722497	4i (1:250)
Antibody	CDT1 (rabbit monoclonal) antibody	CST	Cat. #: 8064; RRID:AB_10896851	4i (1:200)
Antibody	CDC6 (mouse monoclonal) antibody	Santa Cruz	Cat. #: sc-9964; RRID:AB_627236	4i (1:100)
Antibody	Donkey anti-rabbit AlexaFluor Plus 488 (Donkey polyclonal) antibody	Thermo Fisher Scientific	Cat. #: A32790; RRID:AB_2762833	4i (1:500)
Antibody	Donkey anti-goat AlexaFluor plus 647 (Donkey polyclonal) antibody	Thermo Fisher Scientific	Cat. #: A32758; RRID:AB_2762828	4i (1:500)
Antibody	Donkey anti-mouse AlexaFluor Plus 555 (Donkey polyclonal) antibody	Thermo Fisher Scientific	Cat. #: A32773; RRID:AB_2762848	4i (1:500)
Strain, strain background (*Escherichia coli*)	BL21 Competent *Escherishia coli*	NEB	Cat. #: C2530H	
Strain, strain background (*E. coli*)	DH5-α Competent *Escherishia coli*	NEB	Cat. #: C2988J	
Commercial Assay or Kit	GeneJET Plasmid Miniprep Kit	Thermo Fisher Scientific	Cat. #: K0503	
Commercial Assay or Kit	Q5 Site-Directed Mutagenesis Kit (without competent cells)	NEB	Cat. #: E0552S	
Commercial Assay or Kit	Rneasy Plus Mini Kit	QIAGEN	Cat. #: 74134	
Commercial Assay or Kit	SuperScript III First-Strand Synthesis System	Thermo Fisher Scientific	Cat. #: 18080051	

Appendix 1 Continued on next page

Appendix 1 Continued

Reagent type (species) or resource	Designation	Source or reference	Identifiers	Additional information
Commercial Assay or Kit	Dead Cell Apoptosis Kit with Annexin V FITC and PI for flow cytometry	Thermo Fisher Scientific	Cat. #: V13242	
Chemical compound, drug	SSO Advanced Universal SYBR Green Supermix	Bio-Rad	Cat. #: 1725271	
Chemical compound, drug	Bio-Rad Protein Assay Dye Reagent Concentrate	Bio-Rad	Cat. #: 5000006	
Chemical compound, drug	PrestoBlue Cell Viability Reagent	Thermo Fisher Scientific	Cat. #: A13261	
Chemical compound, drug	Calf Intestinal Phosphatase (CIP)	NEB	Cat. #: M0290	
Chemical compound, drug	Clarity ECL Western Blot Substrate	Bio-Rad	Cat. #: 1705060	
Chemical compound, drug	Cyclohexamide	MilliporeSigma	Cat. #: 1810	
Chemical compound, drug	MG132	Selleck Chemicals	Cat. #: S2619	
Chemical compound, drug	MLN4924	Active Biochem	Cat. #: A-1139	
Chemical compound, drug	Glutathione Agarose Resin	GoldBio	Cat. #: G-250-5	
Chemical compound, drug	EZView Red Anti-FLAG M2 Affinity Gel	MilliporeSigma	Cat. #: F2426	
Chemical compound, drug	EZView Red Anti-HA Affinity Gel	MilliporeSigma	Cat. #: E6779	
Chemical compound, drug	PierceTM Protein A/G agarose Beads	Thermo Fisher Scientific	Cat. #: 20421	
Chemical compound, drug	Rnase A	MilliporeSigma	Cat. #: R6513	
Chemical compound, drug	Lipofectamine RNAiMAX	Thermo Fisher Scientific	Cat. #: 13778150	
Chemical compound, drug	PolyJet Transfection Reagent	SignaGen	Cat. #: SL100688	
Chemical compound, drug	Lipofectamine 2000	Thermo Fisher Scientific	Cat. #: 11668019	
Cell line (*H. sapiens*)	293T	ATCC	Cat. #: CRL-3216, RRID:CVCL_0063	
Cell line (*H. sapiens*)	U2OS	ATCC	Cat. #: HTB-96; RRID:CVCL_0042	
Cell line (*H. sapiens*)	HeLa	ATCC	Cat. #: CCL-2; RRID:CVCL_0030	
Cell line (*H. sapiens*)	HeLa sgCTRL	PMID: 27653696		
Cell line (*H. sapiens*)	HeLa sgCCNF	PMID: 27653696		
Cell line (*H. sapiens*)	MCF7 pIND CCNF	This paper		See *Figure 1*, *Figure 1—figure supplement 3*
Cell line (*H. sapiens*)	T47D pIND CCNF	This paper		See *Figure 1*, *Figure 1—figure supplement 3*
Cell line (*H. sapiens*)	NHF-1	William Kaufman Lab (UNC; retired)		

Appendix 1 Continued on next page

Appendix 1 Continued

Reagent type (species) or resource	Designation	Source or reference	Identifiers	Additional information
Cell line (*H. sapiens*)	IMR-90	Yue Xiong Lab (UNC; retired)		
Cell line (*H. sapiens*)	T98G	Tissue Culture Facility, UNC		
Cell line (*H. sapiens*)	NHF-1 doxy-inducible p130 WT	This paper		See *Figure 6*, *Figure 7*, *Figure 5—figure supplements 1 and 2*
Cell line (*H. sapiens*)	NHF-1 doxy-inducible p130 AA	This paper		See *Figure 6*, *Figure 5—figure supplements 1 and 2*
Transfected Construct (*H. sapiens*)	pBABE-p130	Gift from Larisa Litovchick lab (VCU)		For lentiviral transfection
Transfected Construct (*H. sapiens*)	pDEST-HA3-p130	This paper		Transfected construct (human); See *Figures 3–5*, *Figure 4—figure supplement 1*
Transfected Construct (*H. sapiens*)	pDEST-HA3-p130 1–417	This paper		Transfected construct (human); See *Figure 4—figure supplement 1*
Transfected Construct (*H. sapiens*)	pDEST-HA3-p130 418–1139	This paper		Transfected construct (human); See *Figure 4—figure supplement 1*
Transfected Construct (*H. sapiens*)	pDEST-HA3-p130 418-616	This paper		Transfected construct (human); See *Figure 4—figure supplement 1*
Transfected Construct (*H. sapiens*)	pDEST-HA3-p130 418-827	This paper		Transfected construct (human); See *Figure 4—figure supplement 1*
Transfected Construct (*H. sapiens*)	pDEST-HA3-p130 418-1024	This paper		Transfected construct (human); See *Figure 4—figure supplement 1*
Transfected Construct (*H. sapiens*)	pDEST-HA3-p130 828-1139	This paper		Transfected construct (human); See *Figure 4—figure supplement 1*
Transfected Construct (*H. sapiens*)	pDEST-HA3-p130 R658A I660A	This paper		Transfected construct (human); See *Figure 4—figure supplement 1*
Transfected Construct (*H. sapiens*)	pDEST-HA3-p130 R680A L682A	This paper		Transfected construct (human); See *Figure 4—figure supplement 1*
Transfected Construct (*H. sapiens*)	pDEST-FLAG-Cyclin F	PMID: 27653696		Transfected construct (human)
Transfected Construct (*H. sapiens*)	Cyclin F M309A L131A	PMID: 20596027		Transfected construct (human)
Transfected Construct (*H. sapiens*)	pDEST-FLAG-Cyclin F M309A L313A	This paper		Transfected construct (human)
Transfected Construct (*H. sapiens*)	pGEX-GST-p130 593-790	PMID: 9188854		For protein expression in *Escherichia coli*
Transfected Construct (*H. sapiens*)	pGEX-GST-p130 593-790 R680A L682A	This paper		For protein expression in *Escherichia coli*

Appendix 1 Continued on next page

Appendix 1 Continued

Reagent type (species) or resource	Designation	Source or reference	Identifiers	Additional information
Transfected Construct (*H. sapiens*)	pINDUCER20	PMID: 21307310	Addgene #44012; RRID:Addgene_44012	For lentiviral transfection
Transfected Construct (*H. sapiens*)	pINDUCER20 CCNF	This paper		For lentiviral transfection
Transfected Construct (*H. sapiens*)	pLV[Exp]-CMV> Tet3G/ Hygro	VectorBuilder	ID:VB180123-1018bxq	For lentiviral transfection
Transfected Construct (*H. sapiens*)	pLV[TetOn]-Neo-TRE3G > HA/{p130 AA}	this paper, VectorBuilder	ID:VB200319-6469hpy	For lentiviral transfection
Transfected Construct (*H. sapiens*)	pLV[TetOn]-Neo-TRE3G > HA/{p130 WT}	this paper, VectorBuilder	ID:VB200319-6451nqd	For lentiviral transfection
Sequence-based reagent	p130 from AA1 w/attb site Forward	PCR primers		5'-GGGGACAAGTT TGTACAAAAAAG CAGGCTTAAT GCCGTCGGGAGGTGACCAG
Sequence-based reagent	p130 from AA417 w/attb site Reverse	PCR primers		5'-GGGGACCACTTTGTACAA GAAAGCTGGGTA CTACACACAAG GGCTATTCTCCTT
Sequence-based reagent	p130 from AA418 w/attb site Forward	PCR primers		5'-GGGGACAAGTTTGTA CAAAAAAGCAGGCTT AACTCCAGTTTCTACAGCTACG
Sequence-based reagent	p130 from AA 1139 w/attb site Reverse	PCR primers		5'-GGGGACCACTTTGTACAA GAAAGCTGGGTA TCAGTGG GAACCACGGTCATT
Sequence-based reagent	p130 from AA 616 w/attb site Reverse	PCR primers		5'-GGGGACCACTTTGTACAAG AAAGCTGGG TACTAAACTCTGTTT TCATTGTCTCT
Sequence-based reagent	p130 from AA 827 w/attb site Reverse	PCR primers		5'-GGGGACCACTTTGTA CAAGAAAGCTGGG TACTAACTACTGCT GGTTACAGACTG
Sequence-based reagent	p130 from AA 1024 w/attb site Reverse	PCR primers		5'-GGGGACCACTTTGTACAA GAAAGCTGGG TACTAGTACTTCA TGGCAAATGTCTT
Sequence-based reagent	p130 from AA 828 w/attb site Forward	PCR primers		5'-GGGGACAAGTTTGTAC AAAAAAGCAGGCTT AAATAGACCCAGGAAGACCAGC
Sequence-based reagent	p130 R658A I660A Forward	PCR primers		5'-CGCCACATCTCCAA CCACATTATAC
Sequence-based reagent	p130 R658A I660A Reverse	PCR primers		5'-CTGGCTCCAAGT CCTCCAGTATC
Sequence-based reagent	p130 R680A L682A Forward	PCR primers		5'-GGCCTTTGTTGAGAA TGATAGCCCCTC
Sequence-based reagent	p130 R680A L682A Reverse	PCR primers		5'-CGGGCTCTGGTAG TGCTGGCTGG
Sequence-based reagent	Cyclin F from AA 1 w/attb site Forward	PCR primers		5'-GGGGACAAGTTTGTACA AAAAAGCAGGC TTAATGGGGAGCGGCGG CGTGGTCC

Appendix 1 Continued on next page

Reagent type (species) or resource	Designation	Source or reference	Identifiers	Additional information
Sequence-based reagent	Cyclin F from end w/attb site Reverse	PCR primers		5'-GGGGACCACTTT GTACAAGAAAGCTGG GTATTACAGCCTCA CAAGGCCCAGG
Sequence-based reagent	CCNE1 RT-qPCR Forward	PCR primers		5'-AGACATACTTAA GGGATCAGC
Sequence-based reagent	CCNE1 RT-qPCR Reverse	PCR primers		5'-CACACCTCCATTA ACCAATC
Sequence-based reagent	CDC6 RT-qPCR Forward	PCR primers		5'-ATGTAAATCACC TTCTGAGC
Sequence-based reagent	CDC6 RT-qPCR Reverse	PCR primers		5'-GTCATCCTGTT ACCATCAAC
Sequence-based reagent	DHFR RT-qPCR Forward	PCR primers		5'-TTCCAGAAGTCT AGATGATGC
Sequence-based reagent	DHFR RT-qPCR Reverse	PCR primers		5'-CTTCCTTATAAACAGAA CTGCC
Sequence-based reagent	E2F1 RT-qPCR Forward	PCR primers		5'-CTGATGAATATCTGTA CTACGC
Sequence-based reagent	E2F1 RT-qPCR Reverse	PCR primers		5'-CTTTGATCACCATAAC CATCTG
Sequence-based reagent	GAPDH RT-qPCR Forward	PCR primers		5'-GGCCTCCAAGGA GTAAGACC
Sequence-based reagent	GAPDH RT-qPCR Reverse	PCR primers		5'-AGGGGTCTACA TGGCAACTG
Sequence-based reagent	Cyclin F RT-qPCR Forward	PCR primers		5'-AGGACAAGC GCTATGGAGAA
Sequence-based reagent	Cyclin F RT-qPCR Reverse	PCR primers		5'-TCTGTCTTCC TGGAGGCTGT
Sequence-based reagent	CDT1 RT-qPCR Forward	PCR primers		5'-CCTGGGGAAATGGAGAAG
Sequence-based reagent	CDT1 RT-qPCR Reverse	PCR primers		5'-TTGTCCAGCTTGACGTAG
Sequence-based reagent	Cyclin F subcloning into pfastbac Forward	PCR primers		5'-GCTAGGGTCGGATCCAG GAGGCCCCGAAACCTGACC
Sequence-based reagent	Cyclin F subcloning into pfastbac Reverse	PCR primers		3'-GCTAGGCATAGCGGCC GCACCTTAGCTGT CTTGTGTCACT CCTAATGCAGC
Sequence-based reagent	Skp1 subcloning into PGEX-4T-1 Forward	PCR primers		5'-GCTAGGGTCGGA TCCATGCCTT CAATTAAGTTGCAGAG TTCTGATGG
Sequence-based reagent	Skp1 subcloning into PGEX-4T-1 Reverse	PCR primers		3'-GCTAGGCATAGCCTC GAGTTACTT CTCTTCAC ACCACTGGTTCTC
Sequence-based reagent	CCNF #1	siRNA		5'-UAGCCUACCU CUACAAUGAUU
Sequence-based reagent	CCNF #2	siRNA		5'-GCACCCGGU UUAUCAGUAAUU
Sequence-based reagent	siFF	siRNA		5'-CGUACGCGGA AUACUUCGAUU
Other	EdU	Sigma-Aldrich	Cat. #: T511285	For flow cytometry—10 µM to cell media for 30 min prior to fixation
Other	DAPI	Thermo Fisher Scientific	Cat. #: D1306	For flow cytometry (1 µg/ml)

Reagent type (species) or resource	Designation	Source or reference	Identifiers	Additional information
Other	Alexa-Fluor 488 Azide	Thermo Fisher Scientific	Cat. #: A10266	For flow cytometry (0.2 µM)